Int J Earth Sci (Geol Rundsch) (2018) 107:933–953
https://doi.org/10.1007/s00531-017-1511-8

ORIGINAL PAPER

A new U–Pb LA-ICP-MS age of the Rumburk granite (Lausitz Block, Saxo-Thuringian Zone): constraints for a magmatic event in the Upper Cambrian

J. Zieger[1] · U. Linnemann[1] · M. Hofmann[1] · A. Gärtner[1] · L. Marko[2] · A. Gerdes[2]

Received: 27 February 2017 / Accepted: 18 June 2017 / Published online: 3 July 2017

Abstract The basement of the Saxo-Thuringian Zone consists of Upper Neoproterozoic (c. 650-570 Ma) Cadomian arc sediments (Lusatian greywackes) and voluminous intrusions of Early Cambrian granitoids with ages of c. 540 Ma (Lausitz Block and Karkonosze–Izera Massif). The latter basement complexes comprise several c. 505 Ma granites, granodiorites, and gneisses emplaced during the change from a collisional tectonic setting to rift-related geotectonics. We present a new age for the Rumburk granite of 504 ± 3 Ma linking Late Cambrian plutonism at the northern margin of Gondwana with the initial phase of a Cambro–Ordovician rift event. Trace element analysis points to a linkage of the Rumburk granite with other Late Cambrian aged rocks of the Karkonosze–Izera Massif. Furthermore, geochemical data also provide evidence of a melting and recycling of Lusatian greywackes by the intrusion of the Rumburk granite. The youngest age peak of the Rumburk granite at c. 504 Ma is considered to be the age of emplacement. Older inherited age populations at c. 540 and c. 610 Ma are present and likely the result of a melting and recycling of Lusatian granitoids and greywackes. The appearance of Neoproterozoic inheritance and Lu–Hf similarities with the Rumburk granite strongly suggest the Lusatian greywackes as source rocks. There is a significant age gap of c. 35 Ma between Cambrian plutonic and volcanic rocks in Saxo-Thuringia. Hence, we consider two distinct pulses of magmatic activity during the transition from the Cadomian orogeny to the opening of the Rheic Ocean.

Keywords Rumburk granite · Cadomian orogeny · Cambro–ordovician rifting · Lausitz block · Zircon dating

Introduction

The Rumburk granite is named after the northern Czech city of Rumburk and is part of the Cadomian Lausitz Block (Fig. 1). Due to its bluish color and the microcline megacrysts, the Rumburk granite drew early scientific attention (Cotta 1839; Reinisch 1920).

The study area is situated in the Saxo-Thuringian Zone at the northern periphery of the Bohemian Massif and forms the central Variscides (Kossmat 1927; Fig. 1). Field relationships imply an intrusion of the pre-Variscan granitoids among numerous other plutonic rocks the Cadomic sediments and volcanics of the Lausitz Block and the Karkonosze–Izera Massif (Domečka 1970; Opletal et al. 1983). The Cadomian Basement of the Saxo-Thuringian Zone comprises many different rock types due to multiple tectono-metamorphic events along the margin of northern Gondwana in mid-Neoproterozoic and earliest Cambrian (Linnemann et al. 2010a). Terranes, microcontinents, and crustal units, such as Saxo-Thuringia and Iberia, were affected. The opening of an oceanic ridge caused uplifting of the continental crust and subsidence of the upper plate (Linnemann et al. 2007). An emerging heat flow caused a phase of magmatic activity, e.g., the intrusion of the Rumburk granite (Linnemann et al. 2007). This configuration led to a complex and heterogenic composition of the Saxo-Thuringian Zone.

✉ J. Zieger
johannes.zieger@senckenberg.de

[1] Senckenberg Naturhistorische Sammlungen Dresden, Museum für Mineralogie und Geologie, Königsbrücker Landstr. 159, 01109 Dresden, Germany

[2] Institut für Geowissenschaften, Mineralogie, Goethe Universität Frankfurt, Altenhoeferallee 1, 60438 Frankfurt, Germany

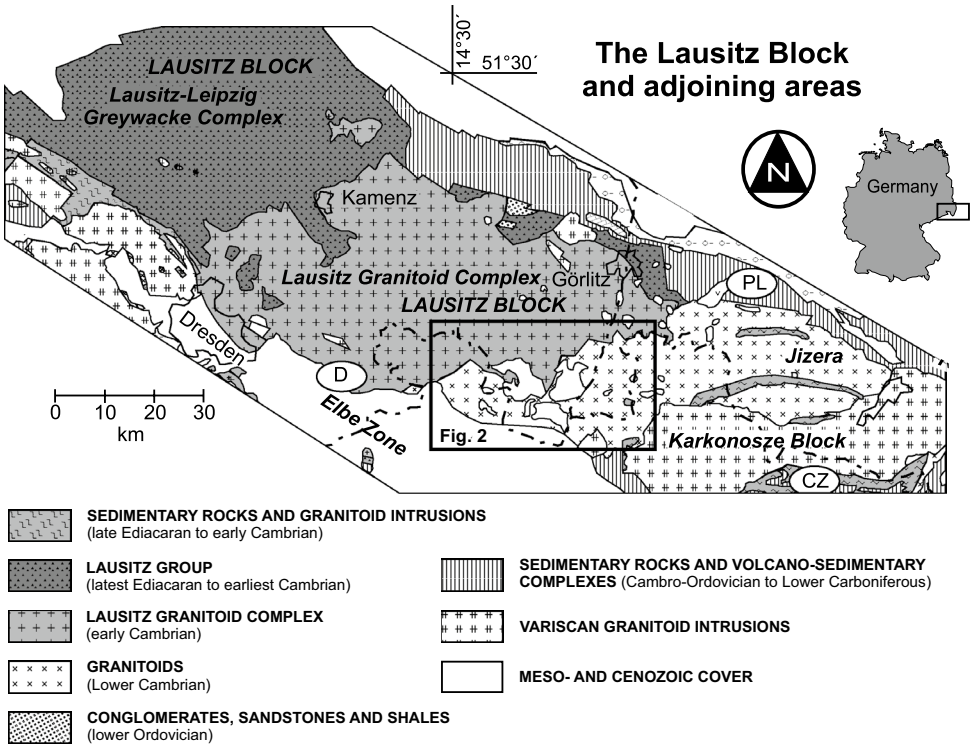

Fig. 1 Geological map of the Cadomian basement of the Lausitz Block (Saxo-Thuringian Zone) including deposits of the Lausitz-Leipzig Greywacke Complex (latest Ediacaran to early Cambrian), Early Cambrian intrusions of the Lausitz Granitoid Complex, and geological units of adjoining areas (map after Linnemann et al. 2007). Working area was situated within the *black rectangle*

The first magmatic event forming the Lausitz Block and the Karkonosze–Izera Massif in the earliest Cambrian was dated at c. 540 Ma (Kröner et al. 1994; Gehmlich et al. 1997; Tichomirowa 2002). A second pulse of magmatic activity is dated at c. 505 Ma (Kröner et al. 1994; Gehmlich et al. 1997; Oberc-Dziedzic et al. 2009), suggesting a significant gap of c. 35 Ma.

In this paper, we present a new age for the Rumburk granite. We compare these new radiometric ages with previously published data to demonstrate the links with other granitoids of the Saxo-Thuringian Zone. Furthermore, we point out potential source rocks which were molten and recycled by the Rumburk granite, based on radiometric and geochemical data. Finally, our data will help to understand the general tectonic setting at the northern margin of Gondwana in late Cambrian times.

Geological setting

The Saxo-Thuringian Zone showcases widespread evidence of alteration during the Cadomian orogeny. This major tectonic event began c. 750 Ma ago and climaxed at the end of the Neoproterozoic to the earliest Cambrian at c. 530 Ma (e.g., Linnemann et al. 2007). At this time the Saxo-Thuringian Zone was a mobile belt situated north of Gondwana. In this zone, only the younger igneous rocks and derived sediments from related magmatic events are preserved (Buschmann 1995; Buschmann et al. 2001; Linnemann et al. 2007). These rocks originated during the period of c. 570–530 Ma and form the so called "Cadomian Basement" (Linnemann et al. 2008a). The basement consists of rocks whose origin is related to the Cadomian orogeny (Linnemann and Buschmann 1995a, b). The sediments of the Cadomian Basement are diverse and consist of turbiditic greywackes, shales, quartzites, and conglomerates. They show a maximum age of deposition of c. 570–545 Ma (Linnemann et al. 2007). Coeval to a post-depositional deformation of the sediments, large plutons intruded the complexes at c. 540–530 Ma, due to an arc-continent collision (Gehmlich 2003, Linnemann et al. 2000, 2007; Tichomirowa et al. 2001).

The Saxo-Thuringian Zone features a number of different volcano-sedimentary units, which are evidence for a volcanic arc-related origin during the Cadomian orogeny. At first the Cadomian back-arc basin opened at c. 580–560 Ma (Linnemann et al. 2007). This passive margin glaciomarine diamictic sequence is made up of greywackes (Linnemann 1991; Linnemann and Romer 2001), whereas the active margin sequence consists of volcano-sedimentary units (Linnemann and Romer 2002). The consequent closure and eventual collision of the arc with the passive margin accompanied with folding and thrusting led to the formation of a retro-arc basin and the subsequent deposition of the Lusatian greywackes in latest Neoproterozoic to earliest Cambrian (545–540 Ma; Linnemann et al. 2007).

The last stage of the Cadomian orogeny in the Saxo-Thuringian Zone was a phase of high magmatic

activity and intrusions of voluminous granitoids at c. 540–530 Ma (e.g. Gehmlich 2003; Zulauf et al. 1999; Tichomirowa et al. 2001; Linnemann et al. 2000). To generate such heat, Linnemann et al. (2007) proposed a possible slab break-off causing this intense phase of magmatism. The ongoing extension of the retro-arc basin led to a thinned and easily intruded crust. During this state, the Lusatian greywackes were molten and recycled by the granitoid magmas, in which they occur as xenoliths (Hammer 1996). The absence of Cadomian high-pressure rocks in Saxo-Thuringia suggests no crustal thickening (Linnemann et al. 2000).

Following on in the Cambrian (c. 530–500 Ma), an asymmetric rift basin comparable to the current Basin and Range Province developed (Nance and Murphy 1996; Nance et al. 2002). The former active margin evolved into a transform margin, which was the beginning of the opening of the Rheic Ocean (Pin and Marini 1993; Nance and Murphy 1996; Kryza and Pin 1997; Nance et al. 2002). During the transition from a collisional to a rift-related setting along the northern margin of Gondwana a second pulse of high magmatism occurred and led to the intrusion of the Rumburk granite and the Izera–Kowary unit of the Karkonosze–Izera Massif (Borkowska et al. 1980; Kröner et al. 1994; Gehmlich et al. 1997; Pin et al. 2007; Oberc-Dziedzic et al. 2009; Białek et al. 2014; Fig. 1). Furthermore, this tectonic regime was confined by the coeval occurrence of the mid-ocean ridge-related Vesser Complex (c. 500 Ma; Bankwitz et al. 1992; Kemnitz et al. 2002; Linnemann et al. 2007). The Vesser Complex may belong to the outer margin of Saxo-Thuringia (Linnemann et al. 2010b) and documents a continental break-up event and a developing intraplate rift (Pin et al. 2007).

The opening of the Rheic Ocean during the latest Cambrian to earliest Ordovician was accompanied by thinning and stretching of the Cadomian crust, eventually leading to an ongoing, expanding rift basin (Linnemann et al. 2007). The Cambro–Ordovician boundary sequence (c. 485 Ma) of the Saxo-Thuringian Zone features numerous volcanic and tuffitic rocks, as a result extensive mid-oceanic ridge volcanism (e.g., Borkowska et al. 1980; Gehmlich 2003; Linnemann et al. 2000; Tichomirowa et al. 2001). This phase of volcanic activity represents the final rift-related magmatism along the northern margin of Gondwana (Linnemann et al. 2007, 2010a).

In some other models, the occurrence of late Cambrian Saxo-Thuringian magmatism is confined to a supra-subduction of a volcanic arc setting (Oliver et al. 1993; Kröner and Hegner 1998; Kröner et al. 1994, 2001), which was situated at the northern margin of Avalonia.

Previous geochronology

There have been numerous ages published for the Rumburk granite and the Izera Massif. The first radiometric age of the Rumburk granite was proposed by Borkowska et al. (1980) with 492 ± 45 Ma (Rb/Sr). A U–Pb age of 493 ± 2 Ma reported by Oliver et al. (1993) is somewhat problematic, due to a reported lead loss. Hence, an age slightly older cannot be excluded. The Izera gneiss dated by Korytowski et al. (1993) gave a U–Pb age of 515 ± 6 Ma. Kröner et al. (1994) proposed a Pb/Pb evaporation age of 571 ± 16 Ma (Ediacaran). Hammer et al. (1999) suggested late Cambrian ages of 490 ± 3 and 494 ± 12 Ma (Pb/Pb single zircon dating). The Izera metagranite dated by Philippe et al. (1995) gave a U–Pb age of 514 ± 5 Ma. More recent studies by Tichomirowa et al. (2001) presented an age for the Rumburk granite of 488 ± 7 Ma, respectively, 486 ± 5 Ma (Pb/Pb evaporation). Żelaźniewicz et al. (2004) obtained U/Pb ages ranging from 533 ± 9 Ma to 548 ± 8 Ma of granodiorites and granodioritic gneisses most likely to be correlated with the granodiorites of the Lausitz Block, not with the younger, Early Cambrian rift-related magmatics. The most recent age of an equivalent for the Rumburk granite was obtained by Białek et al. (2014) with 511 ± 5 Ma (granodiorite, east Lusatia).

The majority of published ages of the Rumburk granite and equivalents range between 480 and 515 Ma, and suggest a connection with the Late Cambrian to earliest Ordovician magmatism high in Saxo-Thuringia. This variation of ages allows no final determination of what the true age of the Rumburk granite is—Late Cambrian or earliest Ordovician (see Geological overview).

Samples

Both samples in our study were taken from the Rumburk granite on the Lausitz Block in eastern Saxony. U–Pb dating was performed on 120 zircons of these samples. U–Pb–Th data and Th/U ratios of igneous and inherited zircon grains from the two investigated granites are presented in Table 1. Sample locations are shown in Fig. 2 and an outcrop photograph is shown in Fig. 3a. Concordia, binned frequency, and probability density distribution plots of all analyzed zircon grains are shown in Figs. 4 and 5.

Sample RG1 (coordinates: N50°57′27.7″; E14°53′11.8″) was collected from the Rumburk granite outcrop near road B66 (Fig. 2). The Rumburk granite intruded the Lausitz Granitoid and Lausitz Greywacke Complexes (Fig. 2). The second sample of Rumburk granite (RG2, coordinates: N50°57′35.5″; E14°53′16.4″)

Table 1 LA-SF-ICP-MS U, Pb, and Th data of single zircon grains of the Rumburk granite. Within each sample, the analyses are sorted by ascending order by ^{206}Pb–^{238}U age for values below 1.0 Ga and by ^{207}Pb–^{206}Pb ages for values above 1.0 Ga

Number	$^{207}Pb^a$ (cps)	U^b (ppm)	Pb^b (ppm)	$\frac{Th^b}{U}$	$\frac{^{206}Pb^c}{^{204}Pb}$	$\frac{^{206}Pb^c}{^{238}U}$	2σ (%)	$\frac{^{207}Pb^c}{^{235}U}$	2σ (%)	$\frac{^{207}Pb^c}{^{206}Pb}$	2σ (%)	rho^d	$\frac{^{206}Pb}{^{238}U}$	2σ (Ma)	$\frac{^{207}Pb}{^{235}U}$	2σ (Ma)	$\frac{^{207}Pb}{^{206}Pb}$	2σ (Ma)	Conc %
RG1_a9	34426	376	27	0.35	479	0.06533	5.2	0.5343	5.5	0.0593	1.9	0.94	408	21	435	20	579	42	70
RG1_b11	41194	318	22	0.08	1058	0.07107	1.9	0.6633	2.1	0.0677	0.9	0.90	443	8	517	9	859	20	52
RG1_a35	12576	541	37	0.12	2035	0.07304	2.7	0.5878	3.4	0.0584	2.1	0.79	454	12	469	13	544	45	84
RG1_b4	31467	233	18	0.29	56032	0.07344	2.0	0.5797	2.8	0.0573	1.9	0.72	457	9	464	10	501	43	91
RG1_b15	33718	243	17	0.10	4169	0.07445	2.0	0.5977	2.4	0.0582	1.3	0.85	463	9	476	9	538	28	86
RG1_b3	29182	213	16	0.11	7664	0.07490	3.0	0.5896	3.3	0.0571	1.4	0.91	466	14	471	13	495	31	94
RG1_b1	31686	259	20	0.26	22784	0.07560	1.8	0.6011	2.2	0.0577	1.2	0.83	470	8	478	8	517	27	91
RG1_b2	17624	134	11	0.28	13777	0.07699	2.2	0.6322	2.7	0.0596	1.6	0.81	478	10	497	11	587	34	81
RG1_a19	5101	98	8	0.39	9090	0.07728	3.7	0.6141	6.1	0.0576	4.9	0.60	480	17	486	24	516	109	93
RG1_a5	29971	379	29	0.12	2591	0.07755	2.7	0.6358	3.0	0.0595	1.3	0.90	482	13	500	12	584	29	82
RG1_a39	13883	574	45	0.14	1375	0.07900	2.7	0.7396	5.1	0.0679	4.3	0.54	490	13	562	22	866	89	57
RG1_a3	47651	542	42	0.03	971	0.07903	2.2	0.6330	3.0	0.0581	2.0	0.75	490	11	498	12	533	43	92
RG1_a38	2922	134	11	0.30	5433	0.07914	3.4	0.6041	4.4	0.0554	2.7	0.78	491	16	480	17	427	61	115
RG1_b13	23772	174	14	0.24	2037	0.07951	3.0	0.6643	3.4	0.0606	1.6	0.89	493	14	517	14	625	34	79
RG1_a8	16558	251	20	0.12	6207	0.08024	2.7	0.6640	3.9	0.0600	2.8	0.69	498	13	517	16	604	61	82
RG1_b7	27343	213	18	0.30	47101	0.08046	1.7	0.6567	2.4	0.0592	1.7	0.70	499	8	513	10	574	37	87
RG1_b20	72625	632	53	0.26	128881	0.08068	2.9	0.6385	3.4	0.0574	1.7	0.86	500	14	501	13	507	38	99
RG1_a28	10230	295	22	0.07	18289	0.08091	2.6	0.6409	3.1	0.0575	1.8	0.83	502	13	503	13	509	39	99
RG1_b10	19853	150	12	0.16	34924	0.08091	1.8	0.6472	2.4	0.0580	1.6	0.76	502	9	507	10	530	35	95
RG1_a14	11593	211	16	0.08	6259	0.08095	2.4	0.6444	3.4	0.0577	2.4	0.71	502	12	505	13	520	52	97
RG1_a40	7575	360	29	0.26	13626	0.08108	2.7	0.6401	4.3	0.0573	3.3	0.63	503	13	502	17	502	73	100
RG1_a10	11226	159	13	0.24	16159	0.08110	4.8	0.6529	5.2	0.0584	1.9	0.93	503	23	510	21	544	42	92
RG1_a33	7375	310	26	0.30	13195	0.08119	2.2	0.6429	3.2	0.0574	2.3	0.69	503	11	504	13	508	50	99
RG1_b8	22803	173	14	0.22	40548	0.08152	1.7	0.6446	2.0	0.0573	1.1	0.84	505	8	505	8	505	24	100
RG1_a13	7834	182	14	0.10	2501	0.08164	3.2	0.6455	3.8	0.0573	2.1	0.84	506	16	506	15	505	45	100
RG1_b19	15271	85	7	0.30	25941	0.08164	2.6	0.6757	3.6	0.0600	2.4	0.74	506	13	524	15	604	53	84
RG1_a17	6875	133	11	0.25	12305	0.08165	3.2	0.6476	4.1	0.0575	2.6	0.77	506	16	507	17	512	58	99
RG1_a31	11404	403	34	0.31	20337	0.08199	2.4	0.6512	2.8	0.0576	1.6	0.83	508	12	509	11	515	34	99
RG1_a36	2992	144	12	0.29	5465	0.08431	2.5	0.6540	3.5	0.0563	2.5	0.70	522	12	511	14	463	56	113
RG1_a21	10254	247	21	0.21	7474	0.08453	2.8	0.6734	3.6	0.0578	2.2	0.80	523	14	523	15	521	47	100
RG1_a20	7777	168	14	0.27	13861	0.08467	2.5	0.6752	3.3	0.0578	2.1	0.76	524	13	524	14	524	46	100
RG1_a2	23657	330	27	0.08	19818	0.08472	2.9	0.6765	3.2	0.0579	1.4	0.90	524	15	525	13	527	31	100
RG1_a4	5488	75	7	0.44	9758	0.08477	2.5	0.6761	3.3	0.0578	2.1	0.77	525	13	524	13	524	46	100
RG1_a23	7721	185	16	0.19	13581	0.08598	3.5	0.6913	4.5	0.0583	2.8	0.78	532	18	534	19	542	62	98

Table 1 continued

Number	$^{207}Pb^a$ (cps)	U^b (ppm)	Pb^b (ppm)	$\frac{Th^b}{U}$	$\frac{^{206}Pb^c}{^{204}Pb}$	$\frac{^{206}Pb^c}{^{238}U}$	2σ (%)	$\frac{^{207}Pb^c}{^{235}U}$	2σ (%)	$\frac{^{207}Pb^c}{^{206}Pb}$	2σ (%)	rho^d	$\frac{^{206}Pb}{^{238}U}$	2σ (Ma)	$\frac{^{207}Pb}{^{235}U}$	2σ (Ma)	$\frac{^{207}Pb}{^{206}Pb}$	2σ (Ma)	Conc %
RG1_a26	11815	320	28	0.32	20883	0.08640	2.3	0.6929	3.0	0.0582	2.0	0.76	534	12	535	13	536	43	100
RG1_a32	4406	168	14	0.26	7756	0.08691	2.6	0.6993	5.4	0.0584	4.7	0.49	537	14	538	23	543	103	99
RG1_a29	8782	240	20	0.06	2511	0.08707	3.4	0.7003	4.2	0.0583	2.6	0.80	538	17	539	18	542	56	99
RG1_b5	24985	126	11	0.33	2795	0.08736	2.0	0.7044	2.5	0.0585	1.5	0.79	540	10	541	11	548	34	99
RG1_a11	10391	179	18	0.58	18237	0.08748	3.3	0.7049	4.2	0.0584	2.6	0.78	541	17	542	18	546	57	99
RG1_a27	20359	452	47	0.64	3799	0.08758	2.9	0.7033	3.6	0.0582	2.1	0.82	541	15	541	15	539	45	100
RG1_b18	30439	217	18	0.03	18829	0.08761	1.9	0.7062	2.3	0.0585	1.1	0.86	541	10	542	10	547	25	99
RG1_b6	25949	159	13	0.10	2113	0.08773	1.8	0.7042	2.8	0.0582	2.2	0.62	542	9	541	12	538	48	101
RG1_a25	6308	155	14	0.21	11066	0.08898	2.7	0.7186	3.4	0.0586	2.0	0.80	549	14	550	14	551	44	100
RG1_b12	19140	141	12	0.10	33162	0.08977	1.7	0.7283	2.8	0.0588	2.2	0.59	554	9	556	12	561	49	99
RG1_a22	7136	161	14	0.13	4290	0.08978	2.4	0.7266	3.7	0.0587	2.8	0.65	554	13	555	16	556	61	100
RG1_a6	14028	193	19	0.42	24494	0.09045	2.5	0.7331	3.3	0.0588	2.1	0.76	558	14	558	14	559	47	100
RG1_a12	6331	112	10	0.28	10988	0.09120	2.7	0.7447	4.9	0.0592	4.0	0.56	563	15	565	21	575	88	98
RG1_a34	8133	166	16	0.11	10300	0.09454	4.3	1.0569	5.5	0.0811	3.5	0.78	582	24	732	29	1223	68	48
RG1_b14	17531	138	14	0.48	9341	0.09470	1.5	0.7682	2.1	0.0588	1.5	0.72	583	9	579	9	561	32	104
RG1_a7	22155	321	31	0.30	2209	0.09499	3.1	0.7783	4.0	0.0594	2.4	0.79	585	18	585	18	583	53	100
RG1_a37	13199	420	41	0.21	289	0.09702	2.6	0.8059	8.9	0.0602	8.5	0.29	597	15	600	41	612	184	97
RG1_a15	19753	344	32	0.11	33764	0.09821	2.3	0.8128	2.8	0.0600	1.5	0.84	604	14	604	13	604	33	100
RG1_b16	163031	391	41	0.10	2770	0.10104	2.9	1.7283	5.6	0.1241	4.8	0.52	621	17	1019	37	2015	85	31
RG1_a16	11968	191	19	0.23	20260	0.10176	3.2	0.8513	3.7	0.0607	1.9	0.85	625	19	625	18	628	42	100
RG1_a1	7147	77	7	0.03	12055	0.10290	2.2	0.8631	3.3	0.0608	2.5	0.67	631	13	632	16	633	54	100
RG1_a30	22389	263	35	0.21	23994	0.12566	2.9	1.6575	4.2	0.0957	3.0	0.70	763	21	992	27	1541	56	50
RG1_a18	9584	62	10	0.18	10338	0.15717	3.6	2.0682	5.7	0.0954	4.5	0.62	941	31	1138	40	1537	84	61
RG1_b17	38945	97	23	0.18	11842	0.22946	2.1	2.7431	3.6	0.0867	2.9	0.57	1332	25	1340	27	1354	57	98
RG1_b9	137550	121	53	0.39	14347	0.39218	1.5	7.3962	2.1	0.1368	1.5	0.72	2133	27	2161	19	2187	25	98
RG2_a17	32887	381	22	0.27	6171	0.05999	2.2	0.47011	3.0	0.05683	2.1	0.72	376	8	391	10	485	46	77
RG2_a43	29962	288	18	0.23	2121	0.06438	2.5	0.54301	3.2	0.06117	1.9	0.79	402	10	440	11	645	42	62
RG2_a42	62159	590	41	0.32	2802	0.06641	2.5	0.53623	2.8	0.05856	1.2	0.90	414	10	436	10	551	27	75
RG2_a53	17726	112	8	0.28	20390	0.06742	2.5	0.54274	3.4	0.05838	2.2	0.74	421	10	440	12	544	49	77
RG2_a23	41159	364	26	0.16	28819	0.07203	2.4	0.56418	2.5	0.05681	0.9	0.94	448	10	454	9	484	19	93
RG2_a40	7775	75	6	0.41	14035	0.07227	2.1	0.56057	3.7	0.05626	3.0	0.58	450	9	452	14	463	67	97
RG2_a3	38125	314	33	0.44	9287	0.07606	2.5	0.61204	3.0	0.05836	1.7	0.83	473	11	485	12	543	37	87
RG2_a52	7410	40	3	0.16	13056	0.07678	3.2	0.61214	4.3	0.05782	2.9	0.73	477	15	485	17	523	64	91
RG2_a11	30046	224	17	0.08	16180	0.08026	2.4	0.63682	2.9	0.05754	1.7	0.82	498	11	500	12	512	37	97
RG2_a60	28955	147	11	0.05	51853	0.08043	2.4	0.63389	3.4	0.05716	2.4	0.72	499	12	499	14	498	53	100

Table 1 continued

Number	$^{207}Pb^{a}$ (cps)	U^{b} (ppm)	Pb^{b} (ppm)	$\frac{Th^{b}}{U}$	$\frac{^{206}Pb^{c}}{^{204}Pb}$	$\frac{^{206}Pb^{c}}{^{238}U}$	2σ (%)	$\frac{^{207}Pb^{c}}{^{235}U}$	2σ (%)	$\frac{^{207}Pb^{c}}{^{206}Pb}$	2σ (%)	rho[d]	$\frac{^{206}Pb}{^{238}U}$	2σ (Ma)	$\frac{^{207}Pb}{^{235}U}$	2σ (Ma)	$\frac{^{207}Pb}{^{206}Pb}$	2σ (Ma)	Conc %
RG2_a28	10289	109	9	0.24	18331	0.08051	2.5	0.63611	3.1	0.05731	1.9	0.79	499	12	500	12	503	42	99
RG2_a26	23955	231	18	0.13	42422	0.08078	2.2	0.64156	2.7	0.05760	1.5	0.82	501	11	503	11	514	34	97
RG2_a15	10166	91	8	0.38	18076	0.08080	2.0	0.63980	2.4	0.05743	1.3	0.85	501	10	502	10	508	28	99
RG2_a4	8978	81	7	0.26	15984	0.08127	2.6	0.64289	3.2	0.05737	1.8	0.83	504	13	504	13	506	40	100
RG2_a16	12792	111	10	0.31	10664	0.08154	2.4	0.64705	3.0	0.05755	1.8	0.80	505	12	507	12	513	40	99
RG2_a47	15566	103	10	0.61	13760	0.08159	2.6	0.64668	3.3	0.05748	2.1	0.78	506	13	506	13	510	46	99
RG2_a19	26530	260	24	0.48	10185	0.08160	2.3	0.64750	2.7	0.05755	1.5	0.84	506	11	507	11	513	32	99
RG2_a6	38491	287	22	0.07	4682	0.08184	2.4	0.64750	3.2	0.05738	2.1	0.76	507	12	507	13	506	45	100
RG2_a9	26657	263	22	0.19	47455	0.08216	2.1	0.65046	2.6	0.05742	1.5	0.81	509	10	509	10	508	34	100
RG2_a46	20098	153	14	0.55	10994	0.08278	2.2	0.65721	2.6	0.05758	1.4	0.85	513	11	513	10	514	30	100
RG2_a50	70693	421	39	0.35	3625	0.08333	2.2	0.70733	3.0	0.06156	2.1	0.72	516	11	543	13	659	45	78
RG2_a44	12310	32	4	0.21	134	0.08357	2.8	1.95210	12.0	0.16942	11.7	0.23	517	14	1099	84	2552	196	20
RG2_a51	26408	170	13	0.06	46628	0.08402	2.1	0.66999	2.6	0.05783	1.5	0.82	520	11	521	11	523	33	99
RG2_a22	5327	44	4	0.33	6916	0.08464	2.2	0.66424	4.0	0.05692	3.3	0.54	524	11	517	16	488	74	107
RG2_a32	40920	457	42	0.37	7875	0.08485	2.4	0.67997	2.7	0.05812	1.2	0.90	525	12	527	11	534	26	98
RG2_a37	25943	268	21	0.06	40440	0.08489	2.2	0.67330	2.6	0.05752	1.4	0.84	525	11	523	11	512	32	103
RG2_a21	19013	188	15	0.11	13085	0.08496	2.1	0.67063	2.5	0.05725	1.4	0.83	526	10	521	10	501	31	105
RG2_a39	25426	257	23	0.33	44768	0.08534	2.3	0.68261	3.2	0.05801	2.2	0.72	528	12	528	13	530	48	100
RG2_a20	13068	107	9	0.26	13007	0.08538	2.2	0.69233	2.6	0.05881	1.3	0.85	528	11	534	11	560	29	94
RG2_a18	25778	232	19	0.09	46005	0.08546	2.2	0.67414	2.8	0.05721	1.6	0.80	529	11	523	11	500	36	106
RG2_a14	7653	67	6	0.27	5122	0.08554	2.8	0.66918	3.9	0.05674	2.7	0.72	529	14	520	16	481	60	110
RG2_a13	28355	225	20	0.32	49928	0.08592	2.7	0.68854	3.0	0.05812	1.4	0.89	531	14	532	13	534	30	99
RG2_a38	9796	96	8	0.20	17336	0.08600	2.4	0.68497	3.2	0.05776	2.0	0.76	532	12	530	13	521	45	102
RG2_a25	12446	102	9	0.25	21806	0.08644	2.2	0.69443	2.7	0.05827	1.5	0.82	534	11	535	11	540	34	99
RG2_a12	15961	138	12	0.15	28242	0.08699	2.2	0.69297	2.9	0.05777	1.9	0.75	538	11	535	12	521	42	103
RG2_a31	9616	94	8	0.12	16795	0.08712	2.9	0.70316	4.4	0.05854	3.4	0.65	538	15	541	19	550	73	98
RG2_a1	13094	109	10	0.29	22940	0.08767	2.3	0.70425	2.6	0.05826	1.1	0.90	542	12	541	11	540	24	100
RG2_a54	8018	37	3	0.18	13912	0.08990	2.5	0.72825	3.4	0.05875	2.3	0.73	555	13	556	15	558	50	99
RG2_a34	57398	576	55	0.30	66715	0.09089	2.9	0.73508	3.0	0.05866	1.0	0.94	561	15	560	13	554	22	101
RG2_a7	6896	51	5	0.36	3225	0.09117	2.7	0.74127	4.1	0.05897	3.1	0.65	562	14	563	18	566	68	99
RG2_a8	10245	64	6	0.21	1061	0.09217	3.1	0.84634	4.4	0.06659	3.2	0.69	568	17	623	21	825	67	69
RG2_a10	15791	112	13	0.68	7933	0.09220	2.4	0.75200	2.8	0.05915	1.6	0.84	569	13	569	12	573	34	99
RG2_a27	16360	136	13	0.21	11594	0.09335	2.3	0.76191	2.8	0.05919	1.6	0.81	575	13	575	13	574	36	100
RG2_a59	28686	137	13	0.16	49389	0.09412	2.1	0.77081	2.6	0.05940	1.6	0.81	580	12	580	12	582	34	100
RG2_a35	18696	159	19	0.70	31683	0.09862	2.4	0.82006	2.8	0.06031	1.5	0.85	606	14	608	13	615	32	99

Table 1 continued

Number	$^{207}Pb^{a}$ (cps)	U^{b} (ppm)	Pb^{b} (ppm)	$\frac{Th^{b}}{U}$	$\frac{^{206}Pb^{c}}{^{204}Pb}$	$\frac{^{206}Pb^{c}}{^{238}U}$	2σ (%)	$\frac{^{207}Pb^{c}}{^{235}U}$	2σ (%)	$\frac{^{207}Pb^{c}}{^{206}Pb}$	2σ (%)	rho[d]	$\frac{^{206}Pb}{^{238}U}$	2σ (Ma)	$\frac{^{207}Pb}{^{235}U}$	2σ (Ma)	$\frac{^{207}Pb}{^{206}Pb}$	2σ (Ma)	Conc %
RG2_a5	22103	138	16	0.46	37447	0.09971	2.6	0.83119	3.5	0.06046	2.3	0.74	613	15	614	16	620	50	99
RG2_a49	8285	44	8	1.81	14245	0.10110	3.4	0.82803	4.0	0.05940	2.1	0.86	621	20	613	19	582	45	107
RG2_a2	22875	138	14	0.23	38524	0.10146	2.4	0.85037	3.0	0.06079	1.8	0.79	623	14	625	14	632	40	99
RG2_a36	25658	254	25	0.09	18999	0.10158	2.7	0.82967	3.3	0.05924	2.0	0.81	624	16	613	15	576	43	108
RG2_a56	17079	81	8	0.04	28534	0.10242	2.3	0.86242	2.9	0.06107	1.9	0.77	629	14	631	14	642	40	98
RG2_a57	24561	63	7	0.22	26483	0.10914	3.4	1.42560	4.4	0.09474	2.9	0.76	668	21	900	27	1523	54	44
RG2_a55	63104	182	22	0.04	83683	0.12274	2.3	1.30253	3.7	0.07697	2.9	0.61	746	16	847	21	1120	58	67
RG2_a48	14701	25	4	0.10	8990	0.12982	58.8	4.07673	90.0	0.22776	68.1	0.65	787	451	1650	1302	3036	1091	26
RG2_a24	43465	106	15	0.17	38930	0.14076	2.8	2.20805	3.4	0.11377	1.9	0.83	849	22	1184	24	1861	34	46
RG2_a33	23404	156	21	0.06	32416	0.14232	2.6	1.44685	3.5	0.07373	2.3	0.74	858	21	909	21	1034	47	83
RG2_a30	43682	155	23	0.10	9093	0.15174	2.3	2.01595	2.8	0.09636	1.7	0.79	911	19	1121	19	1555	32	59
RG2_a45	65180	53	21	0.27	53807	0.36541	2.5	6.23568	2.8	0.12377	1.3	0.90	2008	44	2009	25	2011	22	100
RG2_a29	81921	116	40	0.04	66719	0.34617	2.8	5.98948	3.2	0.12549	1.5	0.88	1916	47	1974	28	2036	27	94
RG2_a41	19658	25	4	0.13	13441	0.17110	2.5	3.52167	3.0	0.14928	1.7	0.83	1018	23	1532	24	2338	29	44
RG2_a58	31030	13	7	0.39	2187	0.46100	1.8	10.14790	3.2	0.15965	2.6	0.57	2444	37	2448	30	2452	45	100

RG1 U–Th–Pb data of magmatic and inherited zircon from sample RG 1, $n = 42$ of 59 measured zircon grains, Rumburk granite, Lausitz Block, Upper Cambrian, Road B66, Kemmlitztal, coordinates: N50°57′27.7″; E14°53′11.8″; height: 275 m

RG2 U–Th–Pb data of magmatic and inherited zircon from sample RG 2, $n = 45$ of 60 measured zircon grains, Rumburk granite, Lausitz Block, Upper Cambrian, abandoned quarry 1 km north of Hirschfelde, coordinates: N50°57′35.5″; E14°53′16.4″; height: 275 m

[a] Within-run background-corrected mean ^{207}Pb signal in counts per second

[b] U and Pb content and Th/U ratio were calculated relative to GJ-1 and are accurate to approximately 10%

[c] Corrected for background, mass bias, laser-induced U–Pb fractionation, and common Pb (if detectable, see analytical method) using Stacey and Kramers (1975) model Pb composition. $^{207}Pb/^{235}U$ calculated using $^{207}Pb/^{206}Pb/(^{238}U/^{206}Pb \times 1/137.88)$. Errors are propagated by quadratic addition of within-run errors (2SE) and the reproducibility of GJ-1 (2SD)

[d] Rho is the error correlation defined as $err^{206}Pb/^{238}U/err^{207}Pb/^{235}$

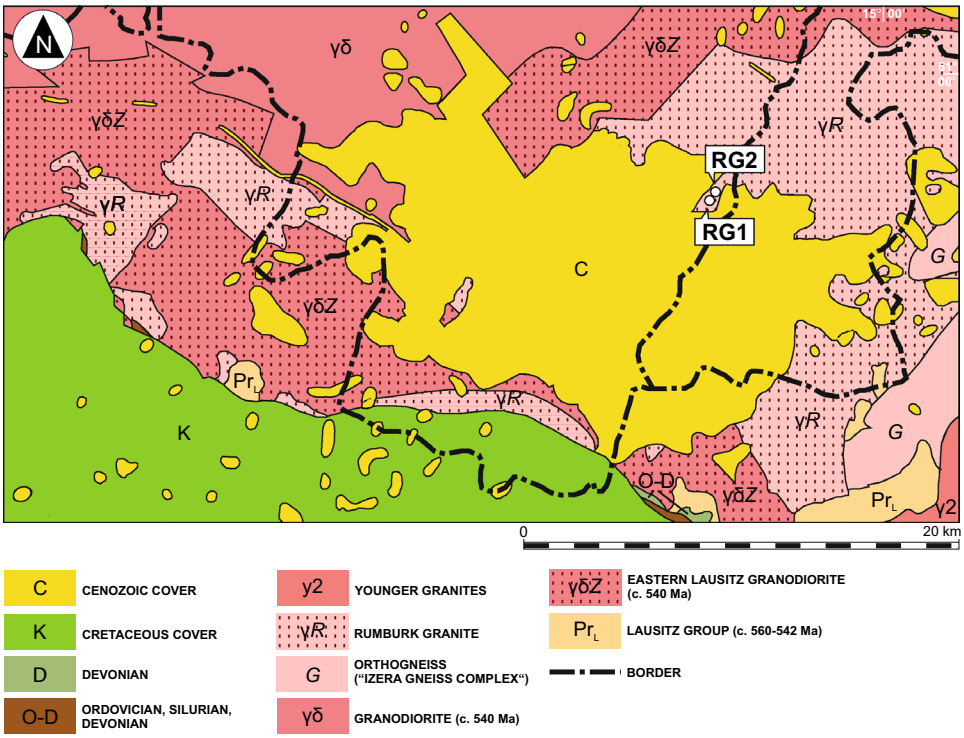

Fig. 2 Geological map of the southeastern Lausitz with indicated sample locations (map after Alexowsky and Leonhardt 1994)

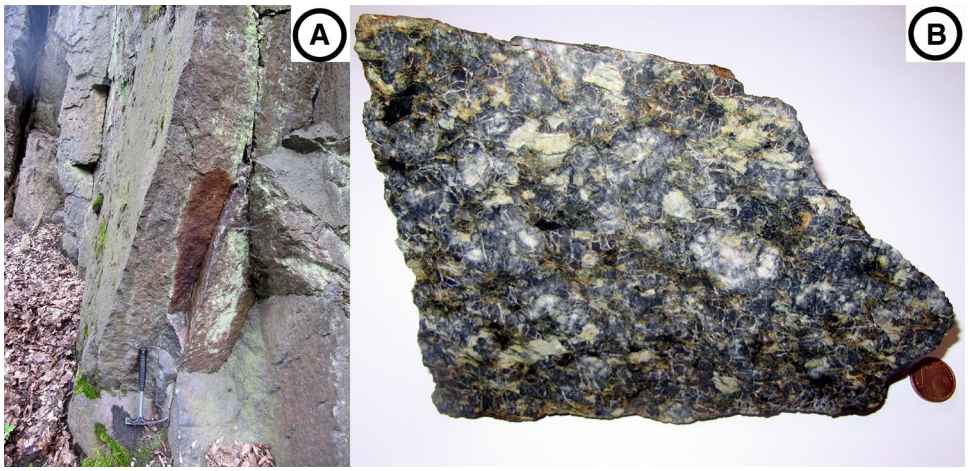

Fig. 3 **a** Outcrop of the location of sample RG2 (N50°57′35.5″ E14°53′16.6″). **b** Polished sample of RG2 with distinguishable quartz and feldspar megacrysts

was collected from an abandoned quarry 1 km north of Hirschfelde (Fig. 2).

The two granite samples are coarse-grained with a hypidiomorphic-granular texture (Fig. 3b). The structure of sample RG2 is unordered with no evidence of a metamorphic alteration, whereas in contrast sample RG1 was collected close to a shear zone. Thus, it is characterized by a gneissic texture. The bluish color of the Rumburk granite is due to cm-sized blue quartz crystals, which have a partly idiomorphic structure. A possible explanation of the blue color is the presence of an overabundance of minute rutile needles, which cause an optical effect (Postelmann 1937). Besides the blue color, microcline megacrysts are typical for the Rumburk granite (Borkowska et al. 1980). The megacrysts are up to 4 cm long. Other components of the matrix include plagioclase (oligoclase or albite) and black to reddish-brown mica (biotite and muscovite) clusters. Unlike the megacrysts, these crystals are only millimeters in length. There are also apatite and magnetite as inclusions.

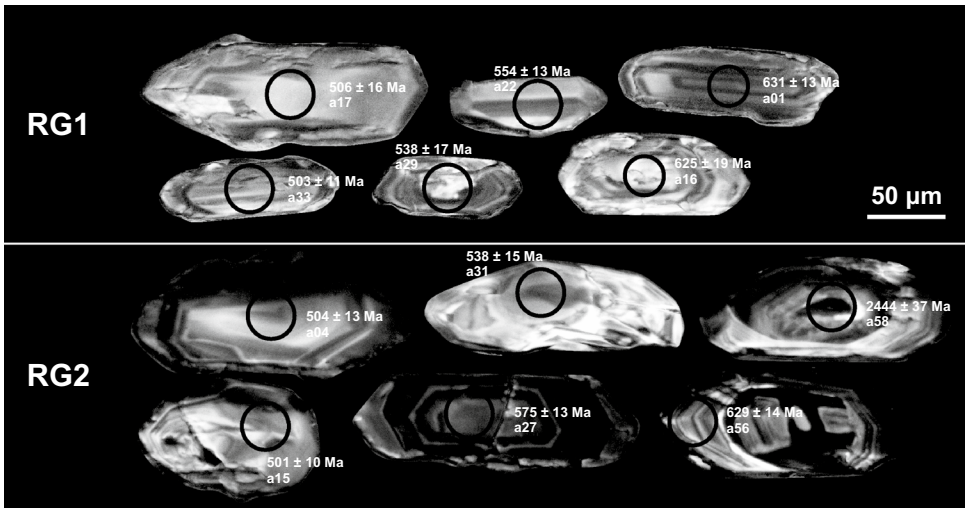

Fig. 4 Selected cathodoluminescence images of zircon grains representing the main age groups for all samples. *Circles* indicating the laser spots with a diameter of 35 and 25 µm. For every spot, the U–Pb age is given with the 2σ error in Ma

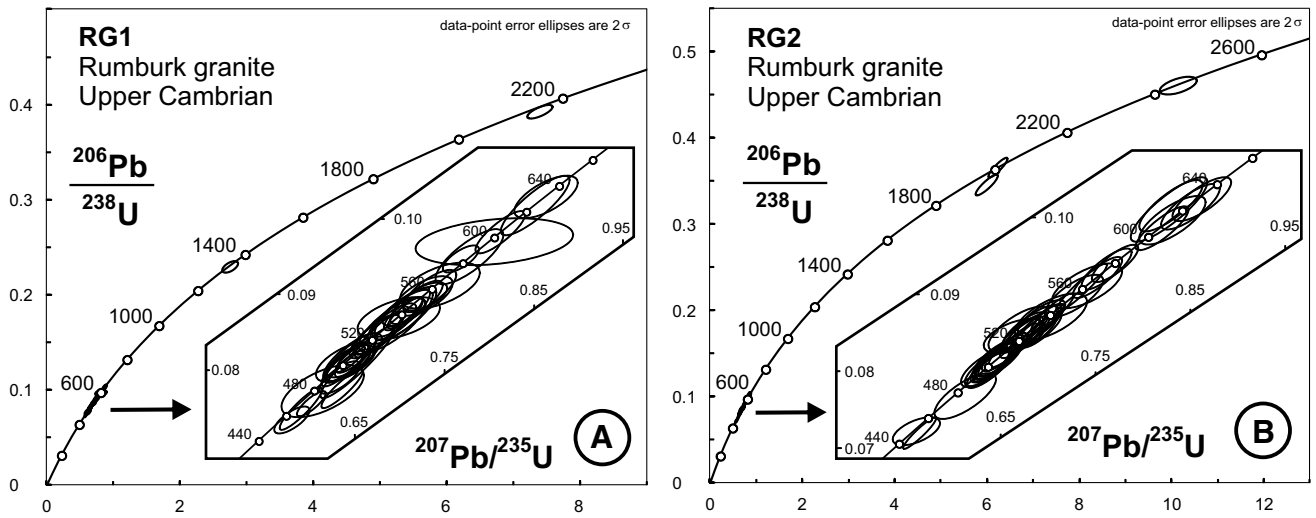

Fig. 5 Concordia plots of all analyzed magmatic zircon grains. **a** Concordia diagram of all measured zircon grains in the range of 400–2500 Ma and of 400–700 Ma (sample RG1, Rumburk granite, Late Cambrian). **b** Concordia diagram of all measured zircon grains in the range of 400–2500 Ma and of 400–700 Ma (sample RG2, Rumburk granite, Late Cambrian)

Methods

Zircon concentrates were separated from 2 to 4 kg sample material at the Senckenberg Naturhistorische Sammlungen Dresden (Museum für Mineralogie und Geologie) using standard methods. Final selection of the zircon grains for U–Pb dating was achieved by hand-picking under a binocular microscope. Zircon grains of all grain sizes and morphological types were selected, mounted in resin blocks, and polished to half their thickness. Zircons were analyzed for U, Th, and Pb isotopes by LA-SF ICP-MS techniques at the Museum für Mineralogie und Geologie (GeoPlasma Lab, Senckenberg Naturhistorische Sammlungen Dresden), using a Thermo-Scientific Element 2 XR sector field ICP-MS (single-collector) coupled to a New Wave UP-193 Excimer Laser System. A teardrop-shaped, low volume laser cell constructed by Ben Jähne (Dresden) and Axel Gerdes (Frankfurt/M.) was used to enable sequential sampling of heterogeneous grains (e.g., growth zones) during time-resolved data acquisition. Each analysis consisted of approximately 15 s background acquisition followed by 30 s data acquisition, using a laser spot-size of 25 and 35 µm, respectively. A common-Pb correction based on the interference- and background-corrected ^{204}Pb signal and a model Pb composition (Stacey and Kramers 1975) was carried out if necessary. The necessity of the correction is judged on whether the corrected ^{207}Pb/^{206}Pb lies outside of the internal errors of the measured ratios (Frei and Gerdes 2009). Discordant analyses were generally interpreted with care. Raw data were corrected for background signal, common Pb,

laser-induced elemental fractionation, instrumental mass discrimination, and time-dependant elemental fractionation of Pb/Th and Pb/U using an Excel® spreadsheet program developed by Axel Gerdes (Institute of Geosciences, Johann Wolfgang Goethe-University Frankfurt, Frankfurt am Main, Germany). Reported uncertainties were propagated by quadratic addition of the external reproducibility obtained from the standard zircon GJ-1 (~0.6% and 0.5–1% for the $^{207}Pb/^{206}Pb$ and $^{206}Pb/^{238}U$, respectively; Jackson et al. 2004) during individual analytical sessions and within-run precision of each analysis. In order to test the accuracy of the measurements and data reduction, we included the Plesovice zircon as a secondary standard in our analyses. Repetitive measurements over the last years of the Plesovice zircon resulted in the age of c. 337 Ma, which fits the results of Slama et al. (2008). Concordia diagrams (2σ error ellipses) and concordia ages (95% confidence level) were produced using Isoplot/Ex 2.49 (Ludwig 2001) and frequency and relative probability plots using AgeDisplay (Sircombe 2004). The $^{207}Pb/^{206}Pb$ age was taken for interpretation for all zircons > 1.0 Ga, and the $^{206}Pb/^{238}U$ ages for younger grains. Further details of the instruments settings are available from Table 1. For further details on analytical protocol and data processing see Gerdes and Zeh (2006). Zircons showing a degree of concordance in the range of 90–102% in this paper are classified as concordant because of the overlap of the error ellipse with the concordia. Concordia ages were derived from analyses with a degree of concordance between 98 and 102%, to exclude led loss effects during age calculation. Th/U ratios are obtained from the LA-ICP-MS measurements of investigated zircon grains. U and Pb content and Th/U ratio were calculated relative to the GJ-1 zircon standard and are accurate to approximately 10%. Analytical results of U–Th–Pb isotopes and calculated U–Pb ages are given in Table 1. The stratigraphic time scale of Gradstein et al. (2012) was used.

Hafnium isotope measurements were taken with a Thermo-Finnigan NEPTUNE multi-collector ICP-MS at Goethe University Frankfurt (Frankfurt/Main) coupled to RESOlution M50 193 nm ArF Excimer (Resonetics) laser system following the method described in Gerdes and Zeh (2006, 2009). Spots of 40 µm in diameter were drilled with a repetition rate of 4.5–5.5 Hz and an energy density of 6 J/cm^2 during 50 s of data acquisition. The instrumental mass bias for Hf isotopes was corrected using an exponential law and a $^{179}Hf/^{177}Hf$ value of 0.7325. In the case of Yb isotopes, the mass bias was corrected using the Hf mass bias of the individual integration step multiplied by a daily $\beta Hf/\beta Yb$ offset factor (Gerdes and Zeh 2009). All data were adjusted relative to the JMC475 of $^{176}Hf/^{177}Hf$ ratio = 0.282160 and quoted uncertainties are quadratic additions of the within-run precision of each analysis and the reproducibility of the JMC475 (2SD = 0.0028%, n = 8). Accuracy and external reproducibility of the method was verified by repeated analyses of reference zircon GJ-1 and Plesovice, which yielded a $^{176}Hf/^{177}Hf$ of 0.282007 ± 0.000026 (2 SD, n = 42) and 0.0282469 ± 0.000023 (n = 20), respectively. This is in agreement with previously published results (e.g., Gerdes and Zeh 2006; Slama et al. 2008) and with the LA-MC-ICP-MS long-term average of GJ-1 (0.282010 ± 0.000025; n > 800) and Plesovice (0.282483 ± 0.000025, n > 300) reference zircon at GUF.

The initial $^{176}Hf/^{177}Hf$ values are expressed as $_{\varepsilon}Hf(t)$, which is calculated using a decay constant value of 1.867 × 10–11 year^{-1}, CHUR after Bouvier et al. (2008; $^{176}Hf/^{177}Hf_{CHUR,today}$ = 0.282785 and $^{176}Lu/^{177}Hf_{CHUR,today}$ = 0.0336) and the apparent Pb–Pb ages obtained for the respective domains (Table 2). For the calculation of Hf two-stage model ages (T_{DM}) in billion years, the measured $^{176}Lu/^{177}Lu$ of each spot (first stage = age of zircon), a value of 0.0113 for the average continental crust, and a juvenile crust $^{176}Lu/^{177}Lu_{NC}$ = 0.0384 and $^{176}Hf/^{177}Hf$ NC = 0.283165 (average MORB; Chauvel et al. 2008) were used.

The geochemical analyses of the rock samples were carried out by FUS-ICP and FUS-MS by Actlabs in Ancaster (Ontario, Canada).

Results

Zircon characteristics

Both samples feature euhedral to subhedral, short-to-normal prismatic zircon crystals with a lengths of 100–250 µm. The grains are transparent, colorless, and show infrequently simple-to-strong zonings in the cathodoluminescence images (Fig. 4). The zircons feature indistinct and irregularly structured interiors. Approximately 10% of the zircon population shows a complex structure with rounded or irregular cores and zoned rims. The zircons are mostly bright in CL.

U–Pb analysis

Analytical results are presented in Figs. 4, 5, 6, 7, 8, 9, 10 and in Table 1. From sample RG1 (Rumburk granite, Lausitz Block), 60 magmatic zircons were analyzed (Table 1). Thirty-two grains show a degree of concordance in the range of 98–102% (Fig. 5a). The youngest concordant grain has an age of 500 ± 14 Ma (Upper Cambrian). The oldest zircon yields an age of 2187 ± 25 Ma. The majority of the sampled zircons (63%) are Cambrian in age, whereas 31% of the grains cluster into the Neoproterozoic range. Only 6% of the sampled zircons yield

Table 2 LA-MC-ICP-MS Lu–Hf isotope data of single zircon grains of the Rumburk granite (Upper Cambrian)

Sample + spot	$^{176}Yb/^{177}Hf$[a]	±2σ	$^{176}Lu/^{177}Hf$[a]	±2σ	$^{178}Hf/^{177}Hf$	$^{180}Hf/^{177}Hf$[b]	Sig_{Hf}[b] (V)	$^{176}Hf/^{177}Hf$	±2σ[c]	$^{176}Hf/^{177}Hf_{(t)}$[d]	$\varepsilon Hf(t)$[d]	±2σ[c]	T_{NC}[e] (Ga)	Age[f](Ma)	±2σ
RG1 (Rumburk granite)															
RG1_a04	0.0753	66	0.00267	18	1.46725	1.88513	7	0.282436	37	0.282410	−1.6	1.3	1.27	525	13
RG1_a06	0.0775	89	0.00282	28	1.46710	1.88704	13	0.282309	32	0.282280	−5.4	1.1	1.50	558	14
RG1_a07	0.0457	38	0.00161	10	1.46721	1.88573	10	0.282431	25	0.282414	−0.1	0.9	1.23	585	18
RG1_a10	0.0677	56	0.00235	15	1.46723	1.88282	8	0.282465	41	0.282443	−0.9	1.4	1.21	503	23
RG1_a11	0.1145	137	0.00364	37	1.46718	1.88571	6	0.282454	62	0.282417	−1.0	2.2	1.24	541	17
RG1_a12	0.0703	62	0.00249	17	1.46717	1.88629	9	0.282384	38	0.282357	−2.6	1.3	1.35	563	15
RG1_a17	0.0692	81	0.00240	24	1.46726	1.88594	10	0.282428	21	0.282405	−2.1	0.7	1.28	506	16
RG1_a31	0.0827	79	0.00293	23	1.46721	1.88601	12	0.282437	23	0.282409	−2.0	0.8	1.27	508	12
RG1_a40	0.0969	102	0.00343	31	1.46721	1.88597	10	0.282459	22	0.282427	−1.5	0.8	1.24	503	13
RG2 (Rumburk granite)															
RG2_a05	0.0764	66	0.00270	18	1.46724	1.88583	7	0.282450	31	0.282419	0.7	1.1	1.21	613	15
RG2_a06	0.0477	43	0.00185	13	1.46719	1.88616	9	0.282538	27	0.282521	2.0	0.9	1.06	507	12
RG2_a09	0.0390	32	0.00150	10	1.46723	1.88574	10	0.281811	34	0.281796	−23.6	1.2	2.45	509	10
RG2_a10	0.1100	115	0.00375	28	1.46719	1.88497	10	0.282473	29	0.282433	0.2	1.0	1.20	569	13
RG2_a12	0.0748	60	0.00277	17	1.46724	1.88513	8	0.282393	37	0.282365	−2.9	1.3	1.35	538	11
RG2_a14	0.0708	61	0.00251	17	1.46718	1.88584	10	0.282418	23	0.282393	−2.1	0.8	1.30	529	14
RG2_a20	0.0481	39	0.00179	11	1.46722	1.88572	10	0.282335	27	0.282318	−4.8	1.0	1.44	528	11
RG2_a23	0.0422	47	0.00155	15	1.46729	1.88524	9	0.282336	45	0.282323	−6.4	1.6	1.47	448	10

Quoted uncertainties (absolute) relate to the last quoted figure. The effect of the inter-element fractionation on the Lu/Hf was estimated to be about 6% or less based on analyses of the GJ-1 and Plesovič zircon. Accuracy and reproducibility were checked by repeated analyses ($n = 12$ and 11, respectively) of reference zircon GJ-1 and Plesovič (data given as mean with 2 standard deviation uncertainties)

[a] $^{176}Yb/^{177}Hf = (^{176}Yb/^{173}Yb)_{true} \times (^{173}Yb/^{177}Hf)_{meas} \times (M_{173(Yb)}/M_{177(Hf)})^{\beta(Hf)}$, $^{\beta}(Hf) = \ln(^{179}Hf/^{177}Hf_{true}/^{179}Hf/^{177}Hf_{measured})/\ln(M_{179(Hf)}/M_{177(Hf)})$, M = mass of respective isotope. The $^{176}Lu/^{177}Hf$ were calculated in a similar way by using the $^{175}Lu/^{177}Hf$ and $^{\beta}(Yb)$

[b] Mean Hf signal in volt

[c] Uncertainties are quadratic additions of the within-run precision and the daily reproducibility of the 40 ppb-JMC475 solution. Uncertainties for the JMC475 quoted at 2SD (2 standard deviation)

[d] Initial $^{176}Hf/^{177}Hf$ and εHf calculated using the apparent Pb–Pb age determined by LA-ICP-MS dating (see column f), and the CHUR parameters: $^{176}Lu/^{177}Hf = 0.0336$, and $^{176}Hf/^{177}Hf = 0.282785$ (Bouvier et al. 2008)

[e] Two-stage model age in billion years using the measured $^{176}Lu/^{177}Hf$ of each spot (first stage = age of zircon), a value of 0.0113 for the average continental crust (second stage), and a depleted mantle $^{176}Lu/^{177}Hf$ and $^{176}Hf/^{177}Hf$ of 0.0384 and 0.283165, respectively

[f] Apparent Pb–Pb age determined by LA-ICP-MS

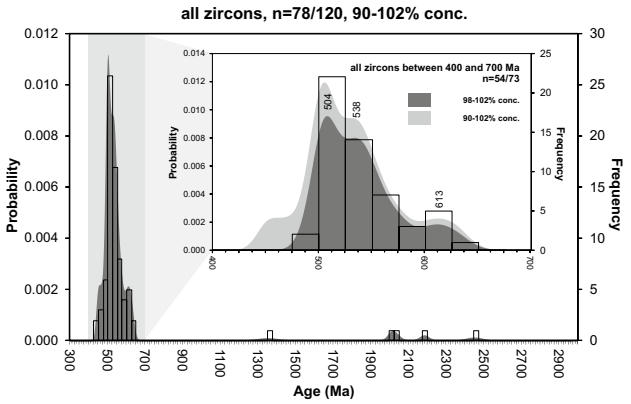

Fig. 6 Combined binned frequency and probability density distribution plots of all analyzed zircon grains of the Rumburk granite

Mesoproterozoic and Paleoproterozoic ages (1360 ± 43, 2187 ± 25 Ma).

From sample RG2 (Rumburk granite, Lausitz Block), 60 magmatic zircons were analyzed (Table 1). Of them, 30 show a degree of concordance in the range of 98–102% (Fig. 5b). The youngest concordant grain yields an age of 499 ± 12 Ma (Late Cambrian). The oldest zircon has an age of 2452 ± 45 Ma (Paleoproterozoic). Like sample RG1, a majority of 57% of all analyzed zircons are Cambrian in age. Only 37% of the grains are Neoproterozoic and 6% of the investigated zircon grains fall into the range of the Paleoproterozoic.

Of the 120 zircon grains analyzed, 62 exhibited a degree of concordance between 98 and 102%. The concordant zircon grains can be divided into several age groups. The main group shows a peak of c. 504 Ma (Series 3; Fig. 6), whereas the age peak of the second largest group is at c. 538 Ma (earliest Cambrian, Fig. 6). There is also a minor Neoproterozoic peak at 613 Ma (Fig. 6). Furthermore, both samples inherit grains with Mesoproterozoic and Paleoproterozoic ages (Fig. 6).

Three complex zircon grains of sample RG1 were analyzed. The rounded cores gave two Neoproterozoic and one Paleoproterozoic age of 563 ± 15, 541 ± 15, and 2133 ± 27 Ma (Fig. 7a–c). In contrast, the younger magmatic rims gave Upper Cambrian ages of 502 ± 12 Ma, respectively, 506 ± 16, 502 ± 13 and 502 ± 9 Ma (Fig. 7a–c).

From sample RG2, two complex zircon grains were analyzed. The two-rounded cores gave one Neoproterozoic age of 613 ± 15 Ma, whereas one Early Cambrian core gave an age of 534 ± 11 Ma (Fig. 7d, e). Like the complex grains of sample RG1, the magmatic rims of sample RG2 gave Late Cambrian ages of 507 ± 12 and 501 ± 11 Ma.

A concordia age calculated for the seven youngest zircon grains of sample RG1 with a concordance between 98 and 102% is at 504 ± 4 Ma (Fig. 8a). The calculated concordia age for sample RG2 for the eleven youngest zircon grains (concordance between 98 and 102%) is at 503 ± 3 Ma (Fig. 8b). The combined age for the 18 youngest zircon grains of both samples is at 504 ± 3 Ma (Fig. 8c).

Th/U and Hf-Analysis

The calculated Th/U ratios are below 1.0 for the majority (82.05%) of all analyzed zircon grains with concordant (90–102%) U–Pb ages, which may point to a felsic melt composition (e.g., Hoskin and Schaltegger 2003; Linnemann et al. 2007). In addition, there is a smaller zircon population of 14 grains (17.95%) with Th/U ratios below 0.1. This is an indicative of a strong metamorphic overprint (Wang et al. 2011). It should be noted that there are no Th/U ratios higher than 0.70 (Fig. 9).

All Lu–Hf isotope data may be found in Table 2. We considered zircons with a degree of concordance between 90 and 102%. The $_{\varepsilon}Hf(t)$ values of 16 Neoproterozoic, Cambrian, and Ordovician zircons from both samples are similar and range from −6.4 to 2.0 with T_{DM} ages between 1000 and 1300 Ma (Fig. 10). Only one measurement (RG2, a09) shows a very low $_{\varepsilon}Hf(t)$ value of −23.6, resulting in a T_{DM} age of 2500 Ma (Paleoproterozoic to Archean). The data suggest that the zircon forming melt was derived from a depleted mantle source mixed with various amounts of older crust. A contamination of the juvenile magma (e.g., island arcs) with Eburnian and even Archean crust is possible.

Geochemical data

All geochemical data are summarized in Table 3. The major element analysis demonstrates that the granites are peraluminous rocks with A/CNK as high as 1.65 (Fig. 11a). The multi-element diagram of the trace elements concentrations normalized to chondrites (Fig. 11b) shows a parallel distribution and strongly suggests a genetic link of both samples. The diagram also displays significant Nb, Sr, and Ti anomalies which point to fractionation processes and/or scarcity of these elements in the source material. The negative Nb anomaly is considered as middle crust material by Wilson (1989). An Nb anomaly is also well developed in the upper crust (Taylor and McLennan 1985). The high negative Sr and Ti anomalies reflect a highly evolved magma and point to a fractionation of plagioclase, apatite, and ilmenite. The

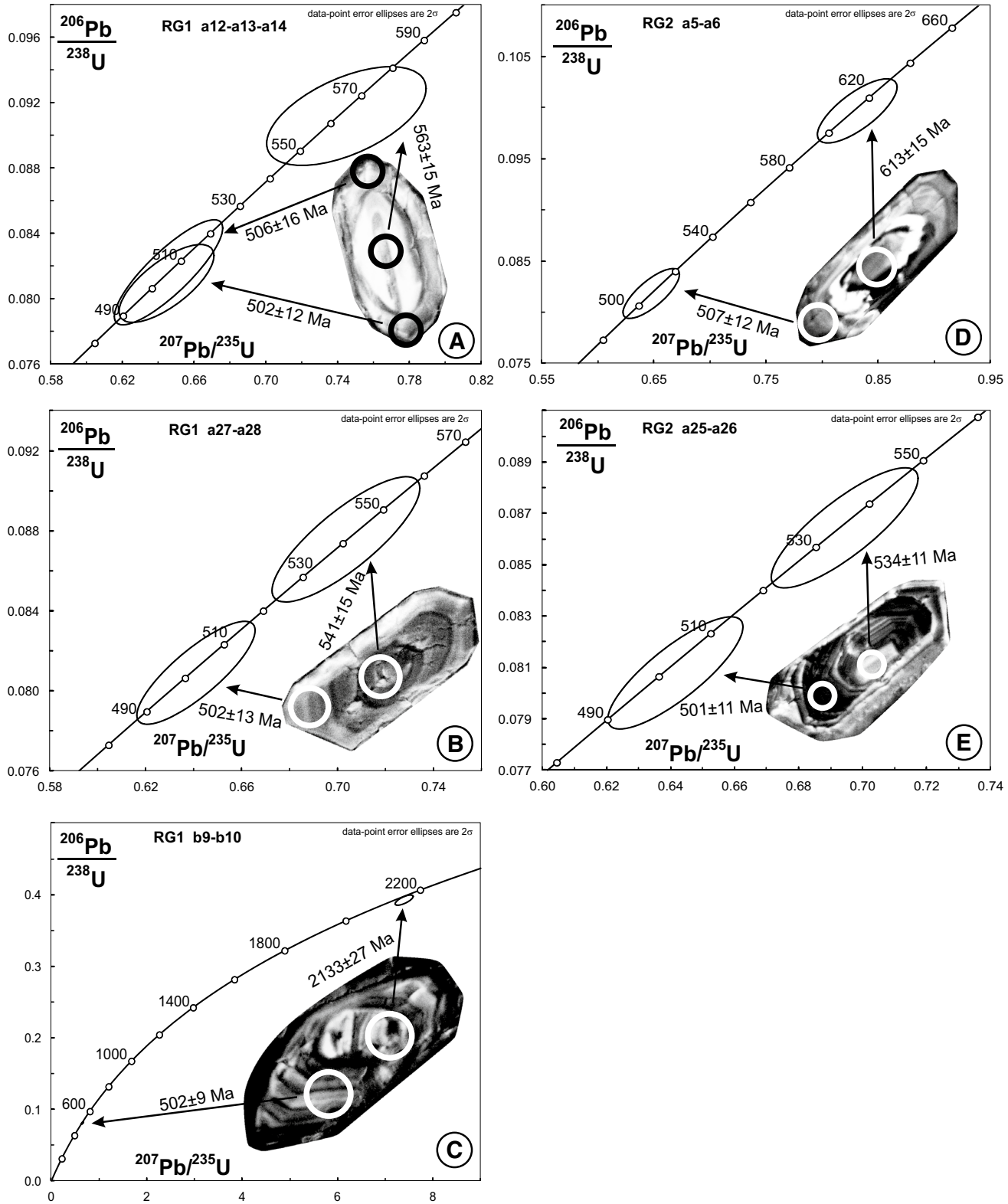

Fig. 7 Concordia plots of complex single zircon grains and its spots. **a** RG1 a12-a13-a14. **b** RG1 a27-a28. **c** RG1 b9-b10. **d** RG2 a5-a6. **e** RG2 a25-a26

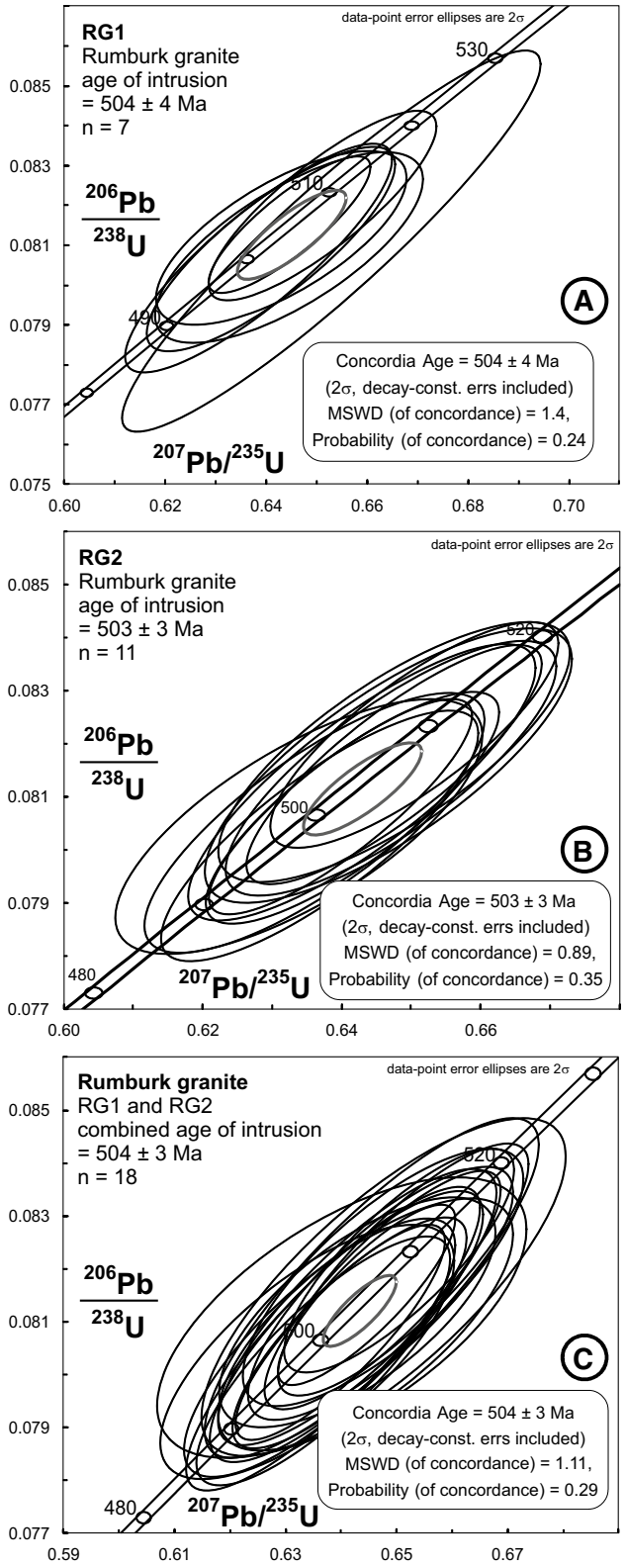

Fig. 8 **a** Concordia plot of the zircon age of the sample RG1. **b** Concordia plot of the zircon age of the sample RG2. **c** Concordia plot of the combined zircon ages of the samples RG1 and RG2

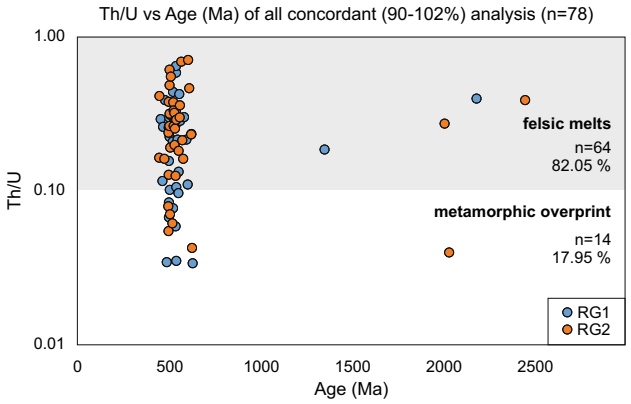

Fig. 9 Th–U versus zircon age diagram of all analyses with a degree of concordance within 90–102%, showing that the majority of zircons were derived from felsic melts. Only a minority of 14 grains show evidence for metamorphic melts (Th–U ratios lower 0.1). The diagram is based on the Th–U ratios given in Table 1

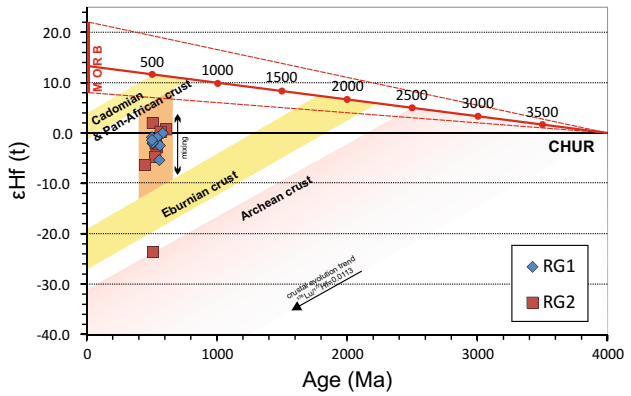

Fig. 10 $_{\varepsilon}$Hf(t) versus age diagram of selected single zircon grains. The continental crust evolution trends of the main components of the West African Craton and the Cadomian orogeny are shown in different colors. See text for discussion

chondrite-normalized plots of the REE of both samples show a strong Eu anomaly (Fig. 11c). The variation of the trace elements and REEs points to a fractional crystallization of plagioclase. The Rb/Y discrimination diagram supports a volcanic arc granite + syncollisional geotectonic setting for the Rumburk granite (Lausitz Block) as well as for seven published analyses of rocks of the Karkonosze–Izera Massif (Fig. 11d). The Hf–Rb/10-Ta*3 and Hf–Rb/30-Ta*3 for the sampled Rumburk granite (Lausitz Block) as well as for seven granitic and metamorphic rocks of the Karkonosze–Izera Massif are plotted in the field of the volcanic arc granite (Fig. 11e, f). This similarity points to a genetic link of the Rumburk granite and Izera gneiss.

Table 3 Major (wt%) and trace element (ppm) whole rock analysis of the Rumburk granite

Sample	RG1	RG2
SiO_2	75.06	73.28
Al_2O_3	12.76	13.06
Fe_2O_3(T)	1.69	2.52
MnO	0.02	0.033
MgO	0.29	0.4
CaO	0.35	0.39
Na_2O	2.68	2.84
K_2O	4.67	4.65
TiO_2	0.126	0.194
P_2O_5	0.2	0.17
LOI	1.2	1.05
Total	99.05	98.57
Sc	4	5
Be	3	3
V	8	14
Cr	30	20
Co	1	2
Ni	<20	<20
Cu	<10	<10
Zn	<30	<30
Ga	21	18
Ge	2	1
As	13	<5
Rb	302	232
Sr	33	46
Y	24	31
Zr	77	90
Nb	6	4
Mo	<2	<2
Ag	<0.5	<0.5
In	<0.1	<0.1
Sn	5	6
Sb	<0.2	<0.2
Cs	5.6	5.1
Ba	128	262
La	14	18.2
Ce	29.1	38.9
Pr	3.51	4.47
Nd	12.2	16.3
Sm	3.3	4
Eu	0.27	0.39
Gd	3.4	4.4
Tb	0.7	0.9
Dy	4.2	5.7
Ho	0.8	1.2
Er	2.4	3.5
Tm	0.41	0.55
Yb	2.8	3.5
Lu	0.44	0.5
Hf	2.3	2.5
Ta	2	1
W	3	1
Tl	1	0.8
Pb	14	16
Bi	<0.1	<0.1
Th	8.9	10.4
U	5.4	4.2

Discussion

Significance of the radiometric ages

In our study, the investigated zircon grains provide a combined U–Pb age of 504 ± 3 Ma for the Rumburk granite (Fig. 8). Both samples overlap in error. Despite that it might be an age of a reworked intrusion, we interpret our calculated age as the time of emplacement for the Rumburk granite. Hence, the new age fits well with other ages obtained from igneous rocks of the Lausitz Block and the Karkonosze–Izera Massif of c. 510–500 Ma (Late Cambrian, Fig. 12).

Our age determined for the Rumburk granite supports the model of three distinct phases of high magmatic activity in Late Cambrian to earliest Ordovician in Saxo-Thuringia (e.g., Gehmlich 2003; Linnemann and Heuse 2000; Linnemann et al. 2000; Kemnitz et al. 2002; Linnemann et al. 2007; Linnemann et al. 2010b). A link with the first magmatic phase in earliest Cambrian (c. 540 Ma; e.g., Linnemann et al. 2000; Tichomirowa et al. 2001; Żelaźniewicz et al. 2009) was discussed by Białek (2003), Kröner et al. (2001), Żelaźniewicz et al. (2003), and Oberc-Dziedzic et al. (2005). In our view, this relationship may be excluded, due to a gap of c. 40 Ma relative to the age of the Rumburk granite. We propose a link with the second magmatic phase (c. 500–510 Ma; Fig. 12), which is confined by the occurrence of several other Early Cambrian granitoids and protoliths of metamorphic rocks of the Lausitz Block and the Karkonosze–Izera Massif. Coeval with the latter magmatics (e.g., Rumburk granite) the MOR-related Vesser Complex developed (Kemnitz et al. 2002; Linnemann et al. 2007; Figs. 12, 13), which is confined as the outer domain of Saxo-Thuringia (Bankwitz et al. 1992), whereas the Lausitz Block and the Karkonosze–Izera Massif represent the inner domain. This illustrates the consequence of a changing tectonic regime from the Cadomian orogeny

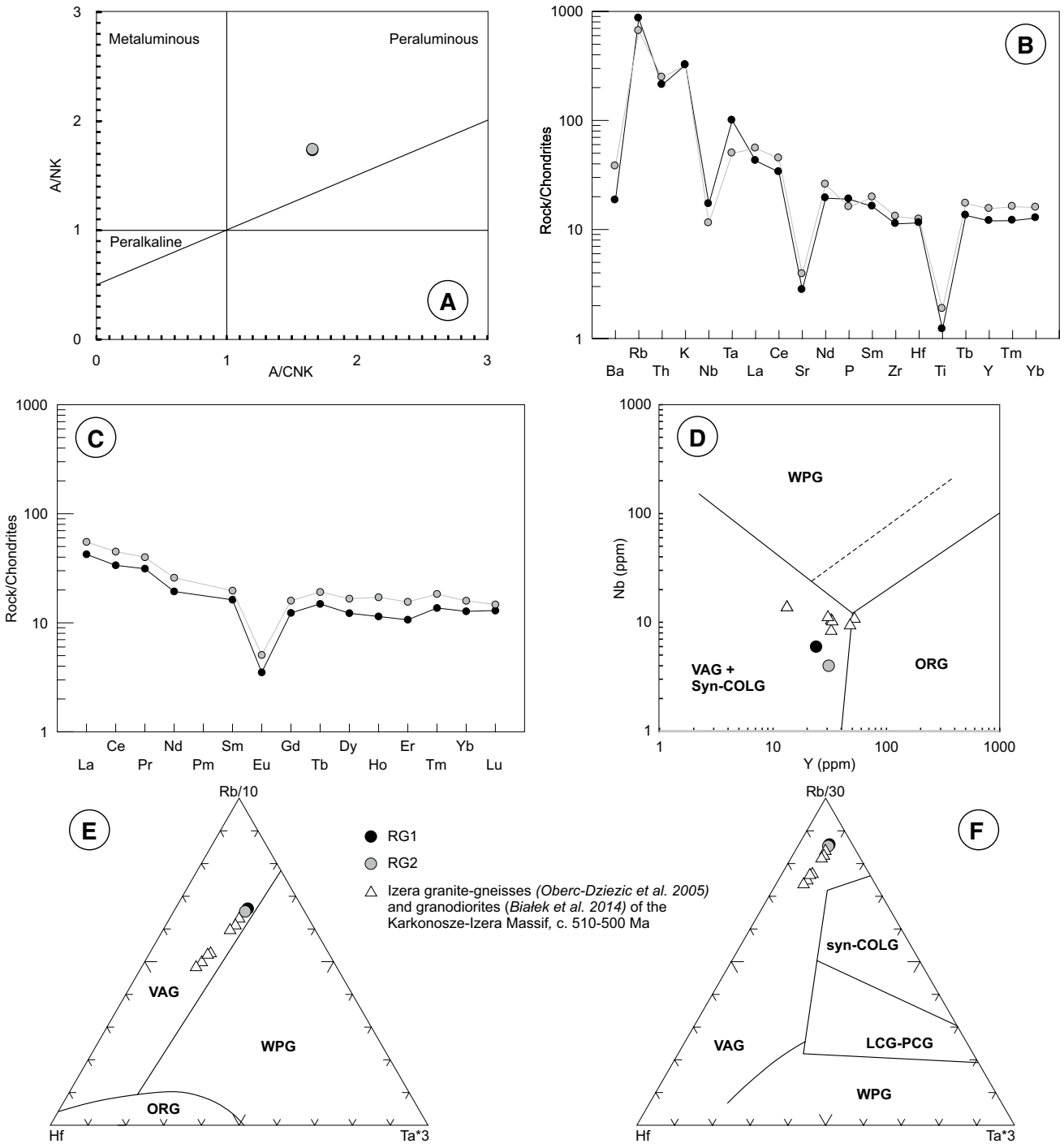

Fig. 11 Plots of geochemical data for samples of the Rumburk granite and Izera gneiss. **a** Aluminousity of both samples (Rumburk granite); Note: both data points lying almost on top of each other. Divisions after Maniar and Piccoli (1989). **b** Chondrite-normalized REE pattern (after Thompson 1982) of both samples showing a negative Nb anomaly. **c** Chondrite-normalized REE patterns (after Nakamura 1974) of both samples. A negative Eu anomaly points to felsic source of the melt. **d** Nb/Y discrimination diagram after Pearce et al. (1984) for the Rumburk granite and selected rocks of the Karkonosze–Izera Massif and the Lausitz Block. **e**, **f** Hf–Rb/10-Ta*3 discrimination diagram after Harris et al. (1986) and Hf–Rb/30-Ta*3 discrimination diagram after Pearce et al. (1984) for both samples as well as for selected rocks of the Karkonosze–Izera Massif. All point to a volcanic arc setting. *VAG* volcanic arc granites, *WAG* within-plate granites, *syn-COLG* syncollisional granites, *ORG* ocean ridge granite, *LCG–PCG* late-collisional–post-collisional granites. Diagrams are based on data given in Table 3

to the Cambro–Ordovician rifting, the initial phase of the opening of the Rheic Ocean. The overlapping Late Cambrian ages suggest that the Rumburk granite and the Izera–Karkonosze Massif intruded into relatively thin transitional crust, separating the oceanic crust (Vesser Complex) from Gondwanan continental crust (Fig. 13). This agrees well with the proposed plate tectonic model for the Late Cambrian (Linnemann et al. 2007, 2010a; Pin et al. 2007; Białek et al. 2014). A relation with the third phase of magmatism in lowermost Ordovician is unlikely because of an age gap of c. 20 Ma (Fig. 12). However, based on the available data, other tectonic models cannot be excluded completely.

Contrary to the proposed geotectonic model, geochemical discrimination diagrams reveal somewhat problematic results. Both analyzed samples, as well as Late Cambrian

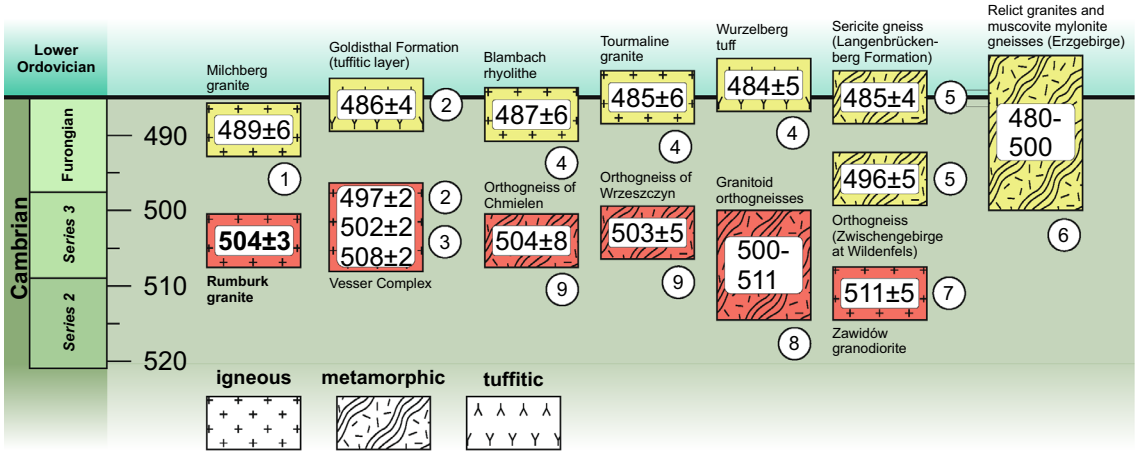

Fig. 12 Generalized lithostratigraphic columns of Late Cambrian volcanic rocks of the Saxo-Thuringian zone. Geochronological data given in Ma (numbered circles): *1* LA-ICP-MS U–Pb (Linnemann & Gerdes, unpubl. data), *2* LA-ICP-MS U–Pb (Linnemann et al. 2007), *3* TIMS U–Pb (Kemnitz et al. 2002), *4* TIMS Pb–Pb (Linnemann et al. 2000), *5* single zircon Pb/Pb evaporation (Gehmlich 2003), *6* single zircon Pb/Pb evaporation (Tichomirowa 2002), *7* SHRIMP U–Pb (Białek et al. 2014), *8* single zircon Pb/Pb evaporation (Kröner et al. 2001), *9* SHRIMP U–Pb (Oberc-Dziedzic et al. 2009)

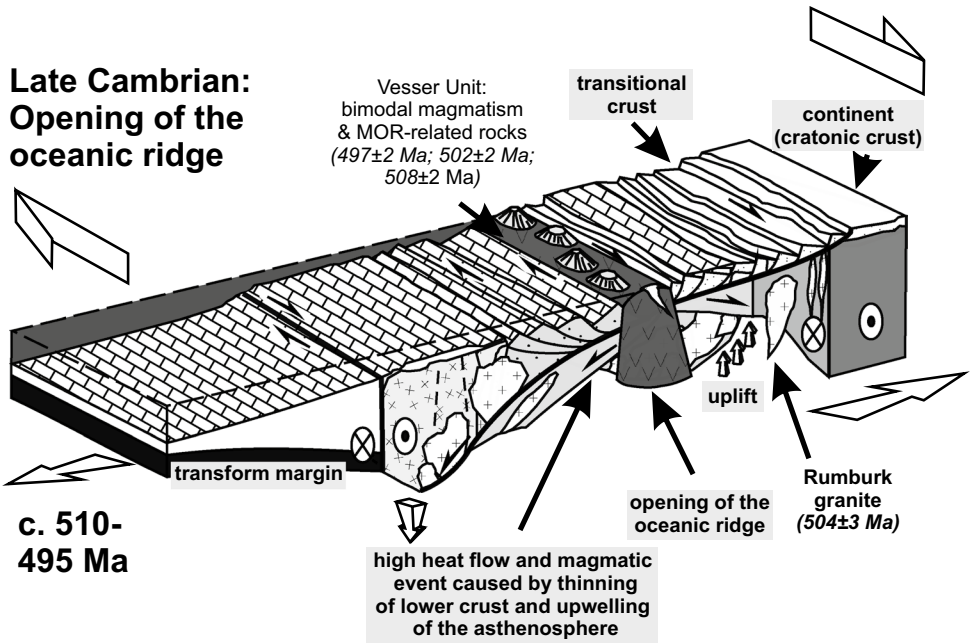

Fig. 13 Plate tectonic model for the opening of the Rheic Ocean during the Late Cambrian between ca. 510 and 495 Ma in the Saxo-Thuringian zone (modified after Linnemann et al. 2007)

samples of the Karkonosze–Izera Massif are volcanic arc granites (Fig. 11d–f). This case was already discussed by Oberc-Dziedzic et al. (2005) and Pin et al. (2007). Both authors pointed out that geochemical discrimination diagrams for granites can be misleading. Granitic magmas mainly reflect the geological setting of their source magma and not the setting of the analyzed rock itself. Hence, source rocks may be volcanic arc-related, but not the resulting rocks (Rumburk granite/Karkonosze–Izera Massif). This was not considered in the model proposed by Kröner et al. (2001), which remains problematic (for further discussion see Oberc-Dziedzic et al. 2005).

Source rocks

Our data suggest that the Rumburk granite intruded rocks similar to the Lusatian granodiorites and greywackes. The geochronological analysis reveals several different age peaks for the Rumburk granite (Figs. 4, 5), similar to inherited zircon ages of the Karkonosze–Izera Massif (Kröner et al. 1994; Białek et al. 2014). These peaks are similar to the age peaks of the Lusatian greywacke (c. 2.4–1.9 Ga and c. 700–560 Ma) also reported by Kröner et al. (1994), Tichomirowa et al. (2001), and Linnemann et al. (2004). The samples we studied yielded inherited zircon grains with Early Cambrian and Neoproterozoic (Ediacaran) ages. In addition, a few Paleoproterozoic grains were recognized. This pattern is characteristic for the West African hinterland as well as for the Cadomian arc and back-arc basin (e.g., Linnemann et al. 2004, 2007; Altumi et al. 2013; Abukabar et al. 2017). A relatively cool magma caused no or only partial melting of the zircons (Fig. 7). Moreover, the multi-element diagram for both samples shows strong Nb, Sr, and Ti anomalies, which are typical for melts of the upper crust (Taylor and McLennan 1985, Fig. 11b). Negative Nb, Sr, and Ti anomalies for the Rumburk granite/Karkonosze–Izera Massif were also obtained by Oberc-Dziedzic et al. (2005), Pin et al. (2007), and Białek et al. (2014). This also suggests a sedimentary source as possible material, similar to the Lusatian greywackes. Furthermore, a strong negative Ti anomaly of the Lower Cambrian rocks indicates a melting and recycling of the Ti-poor Lusatian greywackes by the Rumburk granite (Oberc-Dziedzic et al. 2005; Białek 2007, 2014; Fig. 11b). The observed negative Eu anomaly may point to an advanced plagioclase fractionation during the magma differentiation (e.g., Hammer 1996; Tichomirowa et al. 2001; Oberc-Dziedzic et al. 2005; Pin et al. 2007; Fig. 11c). In addition, the majority of Th/U ratios plot in the field of felsic melt composition (Fig. 9), which points to a crustal source for the Rumburk granite (Hoskin and Schaltegger 2003; Linnemann et al. 2007).

Complex zircon grains of the Rumburk granite inherit cores of c. 540 Ma, which are also evidence for a magmatic event at c. 540 Ma (Fig. 7b, e). Moreover, a distinct age peak at c. 540 Ma (Fig. 6) strongly supports the consideration of a melting and recycling of vast amounts of the possibly slab break-off-induced Lower Cambrian granitoids of the Lausitz Block by the Rumburk granite (e.g., Linnemann et al. 2007; Białek et al. 2014;). In addition, the peraluminousity of the granites gives hints for possible rift-derived source rocks, like the Lusatian greywackes (Philippe et al. 1995; Oberc-Dziedzic et al. 2005; Fig. 11a).

Aside from the single Mesoproterozoic grain, the age population of the Rumburk granite reflects the typical West African magmatic gap from 1000 to 1600 Ma (Linnemann et al. 2008b). A probable source area of the four Paleoproterozoic zircons is the eastern part of the Reguibat Shield, which is dominated by Eburnian rocks (1.8–2.2 Ga) (Ennih and Liegeois 2008; Rocci et al. 1991). A possible source area for Mesoproterozoic zircon ages in Cadomian rocks is the West African Craton, which features Neoproterozoic sediments as well as granites and gneisses with Mesoproterozoic zircon ages (Gärtner et al. 2013, Bradley et al. 2015). Another possible origin of Mesoproterozoic ages is the Amazonian craton, which yields zircon ages of 1.0–1.6 Ga (Schneider Santos et al. 2000). The 25 Neoproterozoic zircon ages (c. 630–570 Ma) recycled by the Rumburk granite are evidence for major orogenic events and crustal growth at the north Gondwana margin as a result of the Cadomian orogeny and are considered to represent the magmatic arc of the Cadomian back-arc basin. Probability density plots fit well with the assumed late-stage basin development in Ediacaran c. 580–560 Ma (Linnemann et al. 2007; Figs. 4, 5).

Furthermore, the obtained Hf data of the Rumburk granite can give hints about the general tectonic setting at the northern margin of Gondwana as well as possible source rocks of the Rumburk granite. All but one $_{\varepsilon}$Hf values of the Rumburk granite give T_{DM} ages of c. 1.0–1.5 Ga (Fig. 10). Hence, in our view this can be explained by a reworking and mixing of Eburnian and Archean crust with juvenile magma of the newly formed Cadomian crust, since no major crustal growth events occurred during Mesoproterozoic. Moreover, no $_{\varepsilon}$Hf values fall into the depleted mantle array, which can be considered as crustal contamination. The lack of high $_{\varepsilon}$Hf values, indicating juvenile magma also hints to a recycling of older (Cadomian) crust (Linnemann et al. 2014). One grain gives a model age of c. 2.5 Ga and can be interpreted as an almost pure reworking of Archean crust. This fits well with the proposed geodynamic setting of the northern margin of Gondwana according to Linnemann et al. (2007). During the developing asymmetric rift basin, magma intruded the thinned transitional crust

and was mixed with older already, Cadomian orogeny induced, mixed continental crust in Early Cambrian.

Conclusions

1. Sample RG1 yielded a youngest U–Pb age of 504 ± 4 Ma, whereas sample RG2 gave a youngest age of 503 ± 3 Ma. The combined age of both samples is 504 ± 3 Ma (Upper Cambrian), which is interpreted as the age of emplacement of the Rumburk granite.
2. Inherited zircon grains of the Rumburk granite clustering at ages of c. 540 Ma indicating an Early Cambrian magmatic high. The obtained Early Cambrian emplacement age for the Rumburk granite (504 ± 3 Ma) suggests a link with the initial opening of the Rheic Ocean. The coeval occurrence of Rumburk granite and Vesser Complex indicating an intrusion of the Rumburk granite into transitional crust, whereas the rift-related rocks of the Vesser Complex represent the outer margin. This follows the proposed transition from the final phase of the Cadomian orogeny to a Cambro–Ordovician rift-related setting at the northern margin of Gondwana. Our data implicate a clear separation of the Late Cambrian magmatic event (c. 505 Ma) from the last phase of high magmatism in uppermost Cambrian to lowermost Ordovician in Saxo-Thuringia (c. 485 Ma).
3. As possible source rocks for the Rumburk granite, we consider rocks like the granitoids of the Lausitz Block and the Lusatian greywackes. A distinct age peak of inherited zircons at c. 540 Ma is characteristic for the intrusions of the late phase of the Cadomian orogeny, which implies a melting and recycling of high amounts of these rocks by the Rumburk granite. Ages of c. 650–570 Ma show a strong similarity with ages obtained from Cadomian back-arc-related sediments. Furthermore an arc-related peraluminousity, most probably representing the geotectonic of the source rock, as well as a characteristic negative Ti anomaly of the Rumburk granite as for the Lusatian greywackes points to a genetic link. Moreover, negative Nd, Sr, and Ti anomalies are evidence for the recycling of upper crust. The few Paleoproterozoic ages may be derived from the West African Craton. In addition, T_{DM} ages of c. 1.0–1.5 Ga are typical for the Cadomian orogen, which may be product of Eburnian and Archean crust mixed with juvenile magma during orogeny and subsequent recycling by the Rumburk granite.

Acknowledgements The authors are grateful to P Vickers-Rich for the revision of the English. The constructive comments and suggestions by F Neubauer and an anonymous reviewer greatly helped to improve the manuscript.

References

Abubaker A, Hofmann M, Gärtner A, Linnemann U, Elicki O (2017) First U–Pb geochronology on detrital zircons from Early-Middle Cambrian strata of the Torgau-Doberlug Syncline (eastern Germany) and palaeogeographic implications. Int J Earth Sci (Geol Rundsch). doi:10.1007/s00531-016-1440-y

Altumi MM, Elicki O, Linnemann U, Hofmann M, Sagawe A, Gärtner A (2013) U–Pb LA–ICP–MS detrital zircon ages from the Cambrian of Al Qarqaf Arch, central-western Libya: provenance of the West Gondwanan sand sea at the dawn of the early Palaeozoic. J Afr Earth Sc 79:74–97

Bankwitz P, Bankwitz E, Kramer W, Pin C (1992) Early Paleozoic bimodal volcanism in the Vesser area, Thuringian Forest, eastern Germany. Zentralblatt für Geologie und Paläontologie Teil I 9(10):1113–1132

Białek D (2003) Cadomian basement of Lusatia. In: Ciężkowski W, Wojewoda J, Żelaźniewicz A (eds) Sudety Zachodnie: od wendu do czwartorzędu. WIND, Wrocaw, pp 33–40

Białek D (2007) Zawidów granodiorite from the Lusatian Massif in SW Poland. In: Kozłowski A, Wiszniewska J (eds) Granitoids in Poland. Arch Mineral Monograph 1, pp 89–99

Białek D, Kryza R, Oberc-Dziedzic T, Pin C (2014) Cambrian Zawidów granodiorites in the Cadomian Lusatian Massif (Central European Variscides): what do the SHRIMP zircon-ages mean? J Geosci 59:313–326

Borkowska M, Hameurt J, Vidal P (1980) Origin and age of Izera gneisses and Rumburk granites in the Western Sudetes. Acta Geol Pol 30:121–145

Bouvier A, Vervoort JD, Patchett PJ (2008) The Lu–Hf and Sm–Nd isotopic composition of CHUR: constraints from unequilibrated chondrites and implications for the bulk composition of terrestrial planets. Earth Planet Sc Lett 273:48–57

Bradley DC, O'Sullivan P, Cosca MA, Motts HA, Horton JD, Taylor CD, Beaudoin G, Lee GK, Ramezani J, Bradley DB, Jones JV, Bowring S (2015) Synthesis of Geological, Structural, and Geochronologic Data (Phase V, Deliverable 53). In: Chapter A of Taylor CD (ed.) Second Projet de Renforcement Institutionnel du Secteur Minier de la République Islamique de Mauritanie (PRISM-II). U.S. Geological Survey Open-File Report 2013-12080-A, p 328

Buschmann B (1995) Geotectonic facies analysis of the Rothstein Formation (Neoproterozoic Saxothuringian Zone, east Germany). Dissertation, TU Bergakademie Freiberg

Buschmann B, Nasdala L, Jonas P, Linnemann U, Gehmlich M (2001) SHRIMP U–Pb dating of tuff-derived and detrital zircons from Cadomian marginal basin fragments (Neoproterozoic) in the northeastern Saxothuringian Zone (Germany). Neues Jahrb Geol P M 6:321–342

Chauvel C, Lewin E, Carpentier M, Arndt NT, Marini JC (2008) Role of recycled oceanic basalt and sediment in generating the Hf-Nd mantle array. Nat Geosci 1:64–67

Cotta B (1839) Erläuterungen zur Section VI der geognostischen Charte des Königreiches Sachsen und der angrenzenden Länderabteilungen. Arnoldische Buchhandlung, Dresden and Leipzig

Domečka K (1970) Pre-Variscan granitoids of the West Sudeten. Sbor Geol Věd Geol 18:161–189

Ennih N, Liegeois J-P (2008) The Boundaries of the West African Craton, with Special Reference to the Basement of the Moroccan Metacratonic Anti-Atlas Belt. Geol Soc London Spec Publ 297:1–17

Frei D, Gerdes A (2009) Precise and accurate in situ U–Pb dating of zircon with high sample throughput by automated LA-SF-ICP–MS. Chem Geol 261:261–270

Gärtner A, Villeneuve M, Linnemann U, El Archi A, Bellon H (2013) An exotic terrane of Laurussian affinity in the Mauritanides and Souttoufides (Moroccan Sahara). Gondwana Res 24:687–699

Gehmlich M (2003) Die Cadomiden und Varisziden des Saxothuringischen Terranes–Geochronologie magmatischer Ereignisse. Freib Forsch C500:1–129

Gehmlich M, Linnemann U, Tichomirowa M, Lützner H, Bombach K (1997) Die Bestimmung des Sedimentationsalters cadomischer Krustenfragmente im Saxothuringikum durch die Einzelzirkon-Evaporationsmethode. Terra Nostra 5:46–49

Gerdes A, Zeh A (2006) Combined U–Pb and Hf isotope LA-(MC-) ICP-MS analysis of detrital zircons: comparison with SHRIMP and new constraints for the provenance and age of an Armorican metasediment in Central Germany. Earth Planet Sci Lett 249:47–61

Gerdes A, Zeh A (2009) Zircon formation versus zircon alteration: new insights from combined U–Pb and Lu–Hf in situ LA-ICPMS analyses, and consequences for the interpretation of Archean zircon from the Central Zone of the Limpopo Belt. Chem Geol 261:230–243

Gradstein FM, Ogg JG, Schmitz MD, Ogg G (eds) (2012) The geologic time scale (Volumes 1 & 2). Elsevier, Amsterdam

Hammer J (1996) Geochemie und Petrogenese der cadomischen und spätvariszischen Granitoide der Lausitz. Freib Forsch C 463:1–107

Hammer J, Eidam J, Röber B, Ehling B-C (1999) Prä-variscischer und variscischer granitoider Magmatismus am NE-Rand des Böhmischen Massivs – Geochemie und Petrogenese. Z geol Wiss 27:401–415

Harris NBW, Pearce JA, Tindle AG (1986) Geochemical characteristics of collision-zone magmatism. Geological Society, London, Special Publications, vol 19, issue 1, pp 67–81

Hoskin PWO, Schaltegger U (2003) The composition of zircon and igneous and metamorphic petrogenesis. In: Hanchar JM, Hoskin PWO (eds.) Zircon. Rev Mineral Geochem 53:27–62

Jackson SE, Pearson NJ, Griffin WL, Belousova EA (2004) The application of laser ablation-inductively coupled plasma-mass spectrometry to in situ U-Pb zircon geochronology. Chem Geol 211:47–69

Kemnitz H, Romer RL, Oncken O (2002) Gondwana Break-up and northern margin of the Saxothuringian belt (Variscides of Central Europe). Int J Earth Sci 91:246–259

Korytowski A, Dörr W, Żelaźniewicz A (1993) U–Pb dating of (meta) granitoids in the NW Sudetes (Poland) and their bearing on tectonostratigraphic correlation. Terra Nova 5 1:331–332 **(Abstract Supplement)**

Kossmat F (1927) Gliederung des vastistischen Gebirgsbaues. Abh Sächsischen Geol Landesamtes 1:1–39

Kröner A, Hegner E (1998) Geochemistry, single zircon ages, and Sm–Nd systematics of granitoid rocks from the Góry Sowie (Owl) mountains, Polish West Sudetes: evidence for early Palaeozoic arc-related plutonism. J Geol Soc London 155:711–724

Kröner A, Hegner E, Hammer J, Haase G, Bielicki KH, Krauss M, Eidam J (1994) Geochronology and Nd-Sr systematics of Lusatian granitoids: significance for the evolution of the Variscan orogen in east-central Europe. Geol Rundsch 83:357–376

Kröner A, Jaeckel P, Hegner E, Opletal M (2001) Single zircon ages and whole-rock Nd isotopic systematics of early Palaeozoic granitoid gneisses from the Czech and Polish Sudetes (Jizerské hory, Krkonoše Mountains and Orlice-Sněžník Complex). Int J Earth Sci 90:304–324

Kryza R, Pin C (1997) Cambrian/Ordovician magmatism in the Polish Sudetes: no evidence for subduction-related setting. EUG 9 Meeting, Strasbourg, Terra Abstracts, p 144

Linnemann U (1991) Glazioeustatisch kontrollierte Sedimentationsprozesse im Oberen Proterozoikum der Elbezone (Weesensteiner Gruppe/Sachsen). Zbl Geo Pal 12(1):2907–2934

Linnemann U, Buschmann B (1995a) Der Nachweis der cadomischen Diskordanz in einer Tiefenbohrung bei Gera und deren Bedeutung für das proterozoisch-paläozoische Standardprofil im Schwarzburger Antiklinorium. Geowiss Mitt Thüringen 3:1–11

Linnemann U, Buschmann B (1995b) Die cadomische Diskordanz im Saxothuringikum (oberkambrisch-tremadocische overlap-Sequenzen). Z Geol Wiss 23(5/6):707–727

Linnemann U, Heuse T (2000) The Ordovician of the Schwarzburg Anticline: geotectonic setting, biostratigraphy and sequence stratigraphy (Saxo-Thuringian Terrane). Z Dtsch Geol Ges 151:471–491

Linnemann U, Romer RL (2001) Geochemical and Nd-Sr-Pb isotopic characterization of Cadomian and Cambro-Ordovician sedimentary rocks with constraints to geotectonic setting and provenance (Saxo-Thuringia, Germany). Schriftenreihe Deutsch Geol Ges (Potsdam)

Linnemann U, Romer RL (2002) The Cadomian orogeny in Saxo-Thuringia, Germany: geochemical and Nd–Sr–Pb isotopic characterization of marginal basins with constraints to geotectonic setting and provenance. Tectonophysics 352:33–64

Linnemann U, Gehmlich M, Tichomirowa M, Buschmann B, Nasdala L, Jonas P, Lützner H, Bombach K (2000) From Cadomian Subduction to Early Paleozoic Rifting: the Evolution of Saxo-Thuringia at the Margin of Gondwana in the Light of Single Zircon Geochronology and Basin Development (Central European Variscides, Germany). Geol Soc Lond Spec Publ 179:131–153

Linnemann U, McNaughton NJ, Romer RL, Gehmlich M, Drost K, Tonk T (2004) West African provenance for Saxo-Thuringia (Bohemian Massif): did Armorica ever leave pre-Pangean Gondwana?—U/Pb-SHRIMP zircon evidence and the Nd-isotopic record. Int J Earth Sci (Geol Rundsch) 93:683–705

Linnemann U, Gerdes A, Drost K, Buschmann B (2007) The continuum between Cadomian orogenesis and opening of the Rheic Ocean: constraints from LA-ICP-MS U–Pb zircon dating and analysis of plate-tectonic setting (Saxo-Thuringian zone, northeastern Bohemian Massif, Germany). Geol S Am S 423:61–96

Linnemann U, Romer RL, Pin C, Aleksandrowski P, Bula Z, Geisler T, Kachlik V, Krzeminska E, Mazur S, Motuza G, Murphy JB, Nance RD, Pisarevsky SA, Schulz B, Ulrich I, Wiszniewska J, Zaba I, Zeh A (2008a) The Precambrian. In: McCann T (ed) The Geology of Central Europe, vol 1. Precambrian and Paleozoic. Geological Society of London, London, pp 21–101

Linnemann U, D'Lemos R, Drost K, Jeffries T, Gerdes A, Romer RL, Samson SD, Strachan R (2008b) Cadomian Tectonics. In: McCann T (ed) The Geology of Central Europe, vol 1. Precambrian and Paleozoic. Geological Society of London, London, pp 103–154

Linnemann U, Romer RL, Gerdes A, Jeffries TE, Drost K, Ulrich J (2010a) The Cadomian Orogeny in the Saxo-Thuringian Zone. In: Linnemann U, Romer RL (eds) Pre-Mesozoic Geology of Saxo-Thuringia—from the Cadomian Active Margin to the Variscan Orogen. Schweizerbart, Stuttgart, pp 37–58

Linnemann U, Hofmann M, Romer RL, Gerdes A (2010b) Transitional stages between the Cadomian and Variscan orogenies: Basin development and tectono-magmatic evolution of the southern margin of the Rheic Ocean in the Saxo-Thuringian Zone (North Gondwana shelf). In: Linnemann U, Romer RL (eds) Pre-Mesozoic Geology of Saxo-Thuringia—from the Cadomian Active Margin to the Variscan Orogen. Schweizerbart, Stuttgart, pp 59–98

Linnemann U, Gerdes A, Hofmann M, Marko L (2014) The Cadomian Orogen: neoproterozoic to Early Cambrian crustal growth and orogenic zoning along the periphery of the West

African Craton—Constraints from U–Pb zircon ages and Hf isotopes (Schwarzburg Antiform, Germany). Precambrian Res 244:236–278

Ludwig KR (2001) Users Manual for Isoplot/Ex rev. 2.49. Berkeley Geochronology Center Special Publication 1a

Maniar PD, Piccoli PM (1989) Tectonic discrimination of granitoids. Geol Soc Am Bull 101:635–643

Nakamura N (1974) Determination of REE, BA, FE, Mg, Na and K in carbonaceous and ordinary chondrites. Geochim Cosmochim Acta 38:757–775

Nance RD, and Murphy JB (1996) Basement isotopic signatures and Neo-proterozoic paleogeography of Avalonian-Cadomian and related terranes in the circum-North Atlantic. In: Nance RD, Thompson MD (eds.) Avalonian and related peri-Gondwanan terranes of the circum-North Atlantic. Geological Society of America Special Paper, vol. 304, pp 333–346

Nance RD, Murphy JB, Keppie JD (2002) A Cordilleran model for the evolution of Avalonia. Tectonophysics 352:1–21

Oberc-Dziedzic T, Pin C, Kryza R (2005) Early Palaeozoic crustal melting in an extensional setting: petrological and Sm–Nd evidence from the Izera granite-gneisses, Polish Sudetes. Int J Earth Sci 94:354–368

Oberc-Dziedzic T, Kryza R, Pin C, Mochnacka K, Larionov A (2009) The Orthogneiss and Schist Complex of the Karkonosze-Izera Massif (Sudetes, SW Poland): U–Pb SHRIMP zircon ages, Nd-isotope systematics and protoliths. Geol Sudet 41:3–24

Oliver GJH, Corfu F, Krogh TE (1993) U-Pb ages from SW Poland: evidence for a Caledonian suture zone between Baltica and Gondwana. J Geol Soc Lond 150:355–369

Opletal M, Domečka K, Vavřín I (1983) Granitoide des Lausitzer Massivs im Südteil des Šluknov Gebiet und ihre neue petrologische Bestimmung. Sbor Geol Věd, Geol 38:141–175

Pearce JA, Harris NBW, Tindle AJ (1984) Trace element discrimination diagrams for the tectonic interpretation of granitic rocks. J Petrol 25:956–983

Philippe S, Haack U, Żelaźniewicz A, Dörr W, Franke W (1995) Preliminary geochemical and geochronological results on shear zones in the Izera-Karkonosze Block (Sudetes, Poland). Terra Nostra 8:122

Pin C, Marini F (1993) Early Ordovician continental break up in Variscan Europe: Nd–Sr isotope and trace element evidence from bimodal igneous associations of the southern Massif Central, France. Lithos 29:177–196

Pin C, Kryza R, Oberc-Dziedzic T, Mazur S, Turniak K, Waldhausrová J (2007) The diversity and geodynamic significance of Late Cambrian (c 500 Ma) felsic anorogenic magmatism in the northern part of the Bohemian Massif: a review based on Sm–Nd isotope and geochemical data. In: Linnemann U, Kraft P, Nance D, Zulauf G (eds.) The Geology of Peri-Gondwana: Avalonian–Cadomian Terranes, Adjoining Cratons, and the Rheic Ocean. Geological Society of America Special Publication, vol. 423, pp 209–230

Postelmann A (1937) Die Ursachen der Blaufärbung gesteinsbildender Quarze. N Jb Mineral Geol Paläont Abt A Beilage 72:401–440

Reinisch R (1920) Erläuterungen zur Geologischen Karte von Sachsen 1:25000, Blatt 87 (Seifhennersdorf-Rumburg) II. Aufl

Rocci G, Bronner G, Deschamps M (1991) Crystalline Basement of the West African Craton. The West African Orogens and Circum-Atlantic Correlatives. Springer, Berlin

Schneider Santos JO, Hartmann LA, Gaudette HE, Groves D, McNaughton NJ, Fletcher IR (2000) A new understanding of the provinces of the Amazon craton based on integration of field mapping and U–Pb and Sm–Nd geochronology. Gondwana Res 3:453–488

Sircombe KN (2004) AGE DISPLAY: an EXCEL workbook to evaluate and display univariate geochronological data using binned frequency histograms and probability density distributions. Comput Geosci 30:21–31

Slama J, Kosler J, Concon DJ, Crowley JL, Gerdes A, Hanchar JM, Horstwood MSA, Morris GA, Nasdala L, Norberg N, Schaltegger U, Schoene B, Tubrett MN, Whitehouse MJ (2008) Plesovice zircon—a new natural reference material for U–Pb and Hf isotopic microanalysis. Chem Geol 249:1–35

Stacey JS, Kramers JD (1975) Approximation of terrestrial lead isotope evolution by a two-stage model. Earth Planet Sci Lett 26:207–221

Taylor SR, McLennan SM (1985) The continental crust: its composition and evolution. Blackwell, Oxford

Thompson RN (1982) Magmatism of the British Tertiary Volcanic Province. Scot J Geol 18:49–107

Tichomirowa M (2002) Zircon inheritance in diatexite granodiorites and its consequence on geochronology—a case study in Lusatia and Erzgebirge (Saxo-Thuringia, eastern Germany). Chem Geol 191:209–224

Tichomirowa M, Berger H-J, Koch EA, Belyatski BV, Götze J, Kempe U, Nasdala L, Schaltegger U (2001) Zircon ages of high-grade Gneisses in the eastern Erzgebirge (Central European Variscides)—constraints on origin of the rocks and Precambrian to Ordovician magmatic events in the Variscan foldbelt. Lithos 56:303–332

Wang X, Griffin WL, Chen J, Huang P, Li X (2011) U and Th Contents and Th/U Ratios of Zircon in Felsic and Mafic Magmatic Rocks: improved Zircon-Melt Distribution Coefficients. Acta Geol Sin 85(1):164–174 **(English Edition)**

Wilson M (1989) Igneous petrogenesis. Unwin Hyman, London

Żelaźniewicz A, Nowak I, Achramowicz S, Czapliński W (2003) The northern part of the Izera-Karkonosze Block: a passive margin of the Saxothuringian terrane. In: Ciężkowski W, Wojewoda J, Żelaźniewicz A (eds) Sudety Zachodnie: od wendu do czwartorzędu. WIND, Wrocaw, pp 17–32

Żelaźniewicz A, Dörr W, Bylina P, Franke W, Haack U, Heinisch H, Schastok J, Grandmontagne K, Kulicki C (2004) The eastern continuation of the Cadomian orogen: U–Pb zircon evidence from Saxo-Thuringian granitoids in south-western Poland and the northern Czech Republic. Int J Earth Sci (Geol Rundsch) 93:773–781

Żelaźniewicz A, Fanning CM, Achramowicz S (2009) Refining the granite, gneiss and schist interrelationships within the Lusatian-Izera Massif, West Sudetes, using SHRIMP U–Pb zircon analyses and new geologic data. Geol Sudet 41:67–84

Zulauf G, Schitter F, Riegler G, Finger F, Fiala J, Vejnar Z (1999) Age constraints on the Cadomian evolution of the Teplá Barrandian unit (Bohemian Massif) through electron microprobe dating of metamorphic monazite. Z Dt Ges Geowiss 150:627–639